



**HAL**  
open science

**Authigenic  $^{10}\text{Be}/^{9}\text{Be}$  ratios and  $^{10}\text{Be}$ -fluxes  
( $^{230}\text{Th}$ -normalized) in central Baffin Bay sediments  
during the last glacial cycle: Paleoenvironmental  
implications**

Quentin Simon, Nicolas Thouveny, Didier Boulès, Laurence Nuttin, Claude  
Hillaire-Marcel

► **To cite this version:**

Quentin Simon, Nicolas Thouveny, Didier Boulès, Laurence Nuttin, Claude Hillaire-Marcel. Authigenic  $^{10}\text{Be}/^{9}\text{Be}$  ratios and  $^{10}\text{Be}$ -fluxes ( $^{230}\text{Th}$ -normalized) in central Baffin Bay sediments during the last glacial cycle: Paleoenvironmental implications. *Quaternary Science Reviews*, 2016, 10.1016/j.quascirev.2016.03.0270277-3791 . hal-01456980

**HAL Id: hal-01456980**

**<https://hal.science/hal-01456980v1>**

Submitted on 6 Feb 2017

**HAL** is a multi-disciplinary open access archive for the deposit and dissemination of scientific research documents, whether they are published or not. The documents may come from teaching and research institutions in France or abroad, or from public or private research centers.

L'archive ouverte pluridisciplinaire **HAL**, est destinée au dépôt et à la diffusion de documents scientifiques de niveau recherche, publiés ou non, émanant des établissements d'enseignement et de recherche français ou étrangers, des laboratoires publics ou privés.

1 **Authigenic  $^{10}\text{Be}/^9\text{Be}$  ratios and  $^{10}\text{Be}$ -fluxes ( $^{230}\text{Th}_{\text{xs}}$ -normalized) in central Baffin Bay**  
2 **sediments during the last glacial cycle: paleoenvironmental implications**

3 Quentin Simon,<sup>1,\*</sup> Nicolas Thouveny<sup>1</sup>, Didier L. Bourlès<sup>1</sup>, Laurence Nuttin<sup>2</sup>, Claude Hillaire-  
4 Marcel<sup>2</sup>, Guillaume St-Onge<sup>2,3</sup>

5 <sup>1</sup>Aix-Marseille Université, CNRS, IRD, CEREGE UM34, 13545 Aix en Provence, France

6 <sup>2</sup>GEOTOP Research Center, H3C3P8 Montréal, Canada

7 <sup>3</sup>Institut des sciences de la mer de Rimouski (ISMER), Canada Research Chair in Marine  
8 Geology, Université du Québec à Rimouski

9 [\\*simon@cerege.fr](mailto:simon@cerege.fr)

10 **Abstract**

11 Authigenic  $^{10}\text{Be}/^9\text{Be}$  ratios and  $^{10}\text{Be}$ -fluxes reconstructed using the  $^{230}\text{Th}_{\text{xs}}$  normalization,  
12 proxies of the cosmogenic radionuclide  $^{10}\text{Be}$  production rate in the atmosphere, have been  
13 measured in a sedimentary core from Baffin Bay (North Atlantic) in order to reconstruct the  
14 geomagnetic dipole moment variations during the last ca. 136 ka BP, and for comparison with  
15 the relative paleointensity (RPI) record derived from paleomagnetic measurements. Our study  
16 revealed that the exchangeable (authigenic)  $^{10}\text{Be}$  measured includes a strong climatic  
17 component related to the glacial dynamics that characterized the circum Baffin Bay during the  
18 last glacial period. Despite normalization applied on the authigenic  $^{10}\text{Be}$  concentrations using  
19 both the scavenged  $^9\text{Be}$  and  $^{230}\text{Th}_{\text{xs}}$  approaches, a strong climatic signal still prevails. Both  
20 normalization methods yield equivalent results that are both strongly correlated with  
21 sedimentological parameters (grain-size and mineralogy). The lower  $^{10}\text{Be}/^9\text{Be}$  ratio values are  
22 associated with coarse-grained carbonate-rich layers while the higher  $^{10}\text{Be}/^9\text{Be}$  ratio values  
23 are found with fine-grained feldspar-rich sediments. This variability is due to both i) sediment  
24 composition control over beryllium-scavenging rates, ii) the glacial history that contributed to  
25 modify the  $^{10}\text{Be}$  concentration in the oceanic realm and notably boundary scavenging  
26 conditions. No pristine geomagnetic field intensity can thus be derived from  $^{10}\text{Be}$   
27 measurements in such a high-variability glacio-marine environment. These results also

28 indicate that the straightforward interpretation of  $^{10}\text{Be}$ -concentration variations as a proxy of  
29 the Interglacial/Glacial (or major interstadials) cycles in Arctic and sub-Arctic regions must  
30 be considered with caution and rather propose to relate  $^{10}\text{Be}$  variations to higher-frequency  
31 paleoclimatic changes and glacial dynamics.

## 32 **1. Introduction**

33 The cosmogenic nuclide Beryllium-10 ( $^{10}\text{Be}$ ) is produced in the stratosphere (~65%) and the  
34 troposphere (~35%) by spallation reactions when highly energetic galactic cosmic rays  
35 interact with nitrogen and oxygen atoms (Lal and Peters, 1967; Dunai and Lifton, 2014). Its  
36 production rate is linked to the Sun and Earth magnetic fields variabilities by a non-linear  
37 inverse relationship (Elsasser et al., 1956; Lal, 1988; Beer et al., 1990; Masarik and Beer,  
38 2009; Kovaltsov and Usoskin, 2010). After its production in the atmosphere,  $^{10}\text{Be}$  is quickly  
39 scavenged onto aerosol particles themselves precipitated (or thrown) within *ca.* 1-3 years into  
40 ocean/continent reservoirs by wet or dry deposition processes (Raisbeck *et al.*, 1981; Beer et  
41 al., 1990; Baroni *et al.*, 2011). Previous studies have shown that -while solar activity inflects  
42 the production rate on shorter timescales-  $^{10}\text{Be}$  flux measured along ice and marine sediment  
43 sequences reflect long term signatures of the geomagnetic dipole moment (Raisbeck *et al.*,  
44 1981, 1985; Yiou *et al.*, 1985; Wagner *et al.*, 2000; Frank et al. 1997; Carcaillet et al., 2003,  
45 2004, Muscheler *et al.* 2004, 2005). The exchangeable- $^{10}\text{Be}$  concentrations (*i.e.*, fraction  
46 adsorbed onto settling particles) measured in the sediments, henceforth referred to the  
47 authigenic  $^{10}\text{Be}$ , are not only reflecting the atmospheric production at the time of their  
48 deposition but also depend on the scavenging rates from the overlying water column, to  
49 advected  $^{10}\text{Be}$  fraction due to oceanic mixing and/or to inherited  $^{10}\text{Be}$  fraction scavenged  
50 during the terrestrial/glacial/meltwater cycling of the carrier particles. Therefore,  
51 normalization of the authigenic  $^{10}\text{Be}$  concentration is a first step in order to remove these  
52 environmental biases and compare  $^{10}\text{Be}$  records with geomagnetic variability.

53 Two methods of normalization have been used in literature: (1) normalization of the  
54 authigenic  $^{10}\text{Be}$  cosmogenic nuclide by the authigenic stable  $^9\text{Be}$  isotope supplied by  
55 terrigenous material entering the ocean (*i.e.*, originating from the dissolution of detrital,  
56 aeolian, riverine and glacier inputs). This method relies on the similar behavior of both  
57 isotopes once homogenized in seawater (Bourlès *et al.*, 1989; Brown *et al.*, 1992). The  
58 authigenic  $^{10}\text{Be}/^9\text{Be}$  ratio method reliably corrects for ocean/continent secondary  
59 contributions and provides robust results clearly demonstrating an inverse relationship with  
60 the geomagnetic field (Henken-Mellies *et al.*, 1990; Robinson *et al.*, 1995; Carcaillet *et al.*,  
61 2003, 2004a, 2004b; Thouveny *et al.*, 2008; Ménabréaz *et al.*, 2011, 2012, 2014; Valet *et al.*,  
62 2014). The second normalization process (2) uses the  $^{230}\text{Th}$ -excess method proposed by  
63 Bacon (1984) to calculate vertical fluxes of any sedimentary component deposited during the  
64 Late Quaternary (see François *et al.*, 2004 for a review) and has been used successfully to  
65 calculate  $^{10}\text{Be}$ -fluxes in numerous studies (*e.g.*, Franck *et al.*, 1997, 2000; Christl *et al.*, 2007,  
66 2010). All these studies notably demonstrate that during periods characterized by low dipole  
67 strength (*i.e.*, corresponding to episodes of collapsed field during reversals or excursions), the  
68 atmospheric  $^{10}\text{Be}$  production rates were significantly larger than during periods with high  
69 dipole strength. Accordingly, the reconstruction of atmospheric  $^{10}\text{Be}$  production rate signals  
70 from marine sedimentary sequences constitutes a complementary approach, independent from  
71 paleomagnetism, to decipher past geomagnetic dipole moment variations. Furthermore, the  
72 comparison between the  $^{10}\text{Be}$  signals from mid-to-low-latitude sites (Ménabréaz *et al.*, 2012,  
73 2014) as well as with recent simulations using general circulation models (GCMs; Heikkilä *et al.*,  
74 2009, 2013) demonstrate a rapid zonal atmospheric mixing of  $^{10}\text{Be}$  before its deposition in  
75 geological archives.

76 In the Arctic Ocean where most dating methods encounter serious limitations, the radioactive  
77 decay rates of the  $^{10}\text{Be}$  measured in marine sediments have been used to establish a Neogene

78 chronostratigraphic framework (assuming a near constant supply of  $^{10}\text{Be}$  in first  
79 approximation) of the ACEX long sedimentary sequence (Frank et al., 2008). Besides,  
80 variations in  $^{10}\text{Be}$  concentrations in Arctic and sub-Arctic sediments have also been used in  
81 order to constrain the stratigraphy of Late Quaternary sedimentary records assuming that  
82 variations of  $^{10}\text{Be}$  concentrations roughly represent Glacial/Interglacial cycles or major  
83 Interstadial periods (Spielhagen et al., 1997, 2004; Sellén et al., 2009; Alexanderson et al.,  
84 2014). In this mechanism, the low  $^{10}\text{Be}$  concentrations corresponding to glacial periods are  
85 caused by a combination of: (1) low inputs of  $^{10}\text{Be}$  due to increased sea ice cover and, (2)  
86  $^{10}\text{Be}$  dilution related to higher accumulation rates of ice rafted debris (IRD); and vice versa  
87 for interglacial (major interstadial) periods.

88 In this study, we present new authigenic  $^{10}\text{Be}/^9\text{Be}$  ratios and  $^{230}\text{Th}_{\text{xs}}$ -normalized  $^{10}\text{Be}$ -fluxes  
89 from a high-latitude marine record (HU2008-029-016PC) from central Baffin Bay and  
90 spanning the last 136 ka. This paper includes a revision of the initial chronostratigraphy of the  
91 core (Simon et al., 2012) in order to improve the robustness of the chronology for the bottom-  
92 half of the core. A primary aim of the study was to examine if  $^{10}\text{Be}$  originating from  
93 continental inputs or advected through oceanic circulation and glacial processes could be  
94 removed from the total authigenic  $^{10}\text{Be}$  concentrations by means of normalization procedures  
95 before any geomagnetic interpretations. We compare the two existing normalization methods  
96 (*i.e.*, authigenic  $^9\text{Be}$  and  $^{230}\text{Th}_{\text{xs}}$ ) using a U and Th-series isotope record from the same core  
97 (Nuttin and Hillaire-Marcel, 2015) and discuss  $^{10}\text{Be}$ -systematics *vs.* sedimentological  
98 parameters, geomagnetic dipole moment variations,  $^{10}\text{Be}$ -fluxes from models and marine/ice  
99 records, and, finally, we discuss its paleoenvironmental implications.

## 100 **2. Environmental setting**

101 Baffin Bay is a subpolar oceanic basin (1300 km long and 450 km wide,  $\sim 690\,000\text{ km}^2$ )  
102 located in the northwest North Atlantic (Figure 1). The bay is one of the main export routes of

103 freshwater from Greenland, the Canadian Arctic and the Arctic Ocean into the North Atlantic  
104 Ocean. Its morphology consists of an elongated abyssal plain (2000–2500 m) surrounded by  
105 the continental shelves of Greenland and Baffin Island. During the glacial periods, the  
106 northeastern Laurentide Ice Sheet (LIS), the Innuitian Ice Sheet (IIS) and the Greenland Ice  
107 Sheet (GIS) formed a nearly continuous and highly dynamic ice belt surrounding Baffin Bay  
108 (Figure 1). On the Greenland side, the GIS extended westward over the inner shelf, and as far  
109 as the shelf edge off Disko Bugt and the Uummannaq Trough during the Last Glacial  
110 Maximum (LGM) (Ó Cofaigh *et al.*, 2012, 2013; Funder *et al.*, 2011). The LIS extended  
111 through Baffin Island, probably as far as its fjord mouths and inlets, and possibly over part of  
112 the Baffin Island shelf during glacial maxima (Margold *et al.*, 2015). In the northern end of  
113 the bay, ice streams in the Smith Sound and Lancaster sounds were particularly large and  
114 active (England *et al.*, 2006; Klassen and Fisher, 1988; Li *et al.*, 2011) and probably  
115 developed into an ice shelf towards the bay (Alley *et al.*, 2010; Marcott *et al.*, 2011).  
116 Numerous studies have demonstrated strong relationships between glacial dynamic, oceanic  
117 circulation and sedimentary processes in the bay (Aksu, 1985, 1987; de Vernal *et al.*, 1987;  
118 Andrews *et al.*, 1998, 2014; Jennings *et al.*, 2014; Simon *et al.*, 2014; Nuttin and Hillaire-  
119 Marcel, 2015). Sedimentation occurs through two main processes: (1) glacial plumes from  
120 lateral sources with large volumes of fine-grained feldspar-rich sediments, which were  
121 transported to the area by sediment-laden supraglacial and subglacial meltwater or nepheloid  
122 layers and (2) Trans-Baffin icebergs drifting from the northern end of the bay with large  
123 volumes of coarse-grained carbonated sediments, leading to the deposition of so-called Baffin  
124 Bay Detrital Carbonate layers (BBDC; Simon *et al.*, 2014).

### 125 3. Material and methods

#### 126 3.1. Core description

127 Core HU2008-029-016PC (70°46.14 N/-64°65.77 W; PC16 hereinafter) was raised from a  
128 2063 m water depth, on the abyssal plain from central Baffin Bay. The 741-cm long core was  
129 retrieved using a piston corer during the 2008-029 CCGS Hudson cruise (Campbell and de  
130 Vernal, 2009). The sediment sequence is mainly composed of a succession of homogeneous  
131 dark gray to olive-gray silty clayey units and of very poorly sorted grayish-brown gravelly  
132 and sandy carbonate-rich layers (dolomite rich, Figure 2). These two lithofacies reflect the  
133 origin, transport and mode of deposition of the lithogenic sediments related to the ice sheet  
134 dynamics evoked above. Moreover, the top of the core down to 20 cm is characterized by  
135 brown to dark brown silty muds while the interval between 120 and 215 cm is constituted by  
136 brownish-black to olive-black clayey muds. These two distinct lithofacies represent sediments  
137 deposited respectively during the Holocene and during marine isotope stage (MIS) 2 (see  
138 Simon *et al.*, 2012, 2014, in prep. and Simon, 2013 for additional information).

#### 139 3.2. Paleomagnetic results and chronology

140 The relative paleointensity (RPI) record previously established by a detailed paleomagnetic  
141 analysis (Simon *et al.*, 2012) reinforced and completed preliminary paleomagnetic results  
142 obtained on a shorter core from the same site (Thouveny 1988). The RPI proxy (Figure 2) is  
143 based on the normalization of the Natural Remanent Magnetization (NRM) with the  
144 Anhyseretic Remanent Magnetization (ARM) over the 25-35 mT AF demagnetization  
145 interval ( $NRM_{25-35mT} / ARM_{25-35mT}$ ). With the exception of few problematic layers, the ARM  
146 normalizer activates the same magnetic assemblages than the NRM, and the RPI proxy  
147 presents no correlation with lithological proxies. Moreover, the derived RPI record was  
148 favorably correlated with RPI reference curves and stacks in order to establish the initial  
149 chronology of the core (Simon *et al.*, 2012). These reference records included mainly the

150 North Atlantic relative paleointensity stack NAPIS-75 (Laj *et al.*, 2000) and the Labrador Sea  
151 core MD95-2024 (Stoner *et al.*, 2000). Two large inclination variations coeval with  
152 paleointensity lows allowing the recognition of two major geomagnetic excursions, *i.e.*, the  
153 Laschamp and Norwegian-Greenland-Sea excursions, and three-radiocarbon ages further  
154 supported the age model (see Simon *et al.*, 2012 for details). This initial chronology is  
155 considered robust for the MIS 2-3-4 periods with a high correlation between PC16 and the  
156 NAPIS-75 stack ( $r=0.82$  between 22-75 ka, Figure 2) and remains unchanged in this study.  
157 For the lower part of the core, large chronological uncertainties (correlation coefficients with  
158 reference records  $<0.51$ ) required revision in order to improve its resolution and to compare  
159  $^{10}\text{Be}$  production rate variations with references. Therefore, the chronology of core PC16 was  
160 updated by tuning the PC16 RPI curve with the ODP 1063 RPI record (Channel *et al.*, 2012)  
161 using 13 tie points ( $r=0.70$  between 75-136 ka, Figure 2). The age model for ODP Site 1063  
162 was constructed by tandem correlation of oxygen isotope and RPI data to calibrated reference  
163 templates using the Match protocol (Lisiecki and Lisiecki, 2002), improving its reliability.  
164 The revised age model offers a significantly improved statistical robustness and places the  
165 PC16 core bottom (741 cm) in the MIS 6 interval representing a 20 ka age shift from the  
166 Simon *et al.* (2012) age model. Using this refined age model, the average sedimentation rate  
167 for the sedimentary sequence is 5.4 cm/ka and presents large variability mainly related to  
168 glacial/deglacial history. The mean sedimentation rates during the Holocene (0-10.6 ka),  
169 Deglacial-peak (10.7-12 ka) and last Glacial (12.1-136.7 ka) periods are 1.9 cm/ka, 25.8  
170 cm/ka and 5.5 cm/ka, respectively (Figure 8).

### 171 3.3. Sample preparation

172 Based on the paleomagnetic record and on U and Th-series isotope records, 76 subsamples of  
173 ~1 g (dry sediment) were collected along core PC16 and processed for the Be isotope analysis  
174 at the CEREGE National Cosmogenic Nuclides Laboratory (France) according to the



175 chemical procedure set-up by Bourlès *et al.* (1989) and summarized in Carcaillet *et al.* (2003,  
176 2004a, 2004b) and Ménabréaz *et al.* (2011, 2012, 2014). The method is detailed here since the  
177 separation procedure has been modified prior to the AMS measurements.  $^{10}\text{Be}$  and its stable  
178 isotope  $^9\text{Be}$  were co-extracted from the authigenic phase of the sediments using 20 ml.g<sup>-1</sup>  
179 sediment of 0.04 M hydroxylamine (NH<sub>2</sub>OH-HCl) in a 25% acetic acid leaching solution at  
180  $95 \pm 5^\circ\text{C}$  for 7 hrs. A 2 ml aliquot of the resulting leaching solution was sampled for the  
181 measurement of the natural  $^9\text{Be}$  concentration. The remaining solution was spiked with 300 µl  
182 of a  $9.8039 \cdot 10^{-4}$  g.g<sup>-1</sup>  $^9\text{Be}$ -carrier before the chemical extraction in order to accurately  
183 determine  $^{10}\text{Be}$  sample concentrations from the measured  $^{10}\text{Be}/^9\text{Be}$  ratios. The Be-purification  
184 was realized by chromatography in two stages. Before each separation stages, the samples  
185 were evaporated and then dissolved in ultra-pure HCl. Be oxy-hydroxides were precipitated at  
186 pH 8.5 from the solution by adding NH<sub>3</sub>. The precipitate was separated by centrifugation,  
187 dissolved in ultra-pure HCl and then loaded onto an exchange column. The iron (Fe) and  
188 manganese (Mn) were separated using a Dowex® 1x8 (100–200 mesh) anion-exchange resin.  
189 The resin was first rinsed with 20 ml MilliQ water and conditioned with 20 ml 10.2 M HCl.  
190 The sample was then loaded onto the column and the Be fraction was collected immediately  
191 using 20 ml 10.2 M HCl for elution. The next purification step was carried out on a Dowex®  
192 50x8 (100–200 mesh) cation-exchange resin in order to separate the Bore (B) and Aluminum  
193 (Al). The resin was rinsed with 30 ml MilliQ water and then conditioned with 30 ml 1 M HCl.  
194 After sample loading onto the column, the B and Be were eluted successively within the first  
195 40 ml and next 120 ml of 1 M HCl eluent while the Al remained trapped within the column.  
196 After the two separation stages, Be oxy-hydroxides were precipitated at pH 8.5 from the final  
197 solution by adding NH<sub>3</sub>. The precipitate was separated by centrifugation, rinsed by re-  
198 suspension using pH 8.5 buffered MilliQ water and centrifugated again. The purified Be oxy-  
199 hydroxides were solubilized in HNO<sub>3</sub> and the resulting solution was transferred into a quartz

200 crucible where it was gently evaporated to dryness at 200°C. Finally, the Be oxy-hydroxides  
201 deposit was oxidized and converted to BeO by heating at 800°C for 1 hr. The BeO was then  
202 mixed with Nb powder and pressed into a cleaned Ti cathode-holder in order to condition the  
203 samples for AMS measurements. In addition to sample processing, several routine blanks and  
204 2 replicates were measured in order to assess both cleanliness and reproducibility during the  
205 chemical extraction.

### 206 3.4. Measurements

207 The natural authigenic  $^9\text{Be}$  concentrations were measured using a graphite-furnace Atomic  
208 Absorption Spectrophotometer (AAS) with a double beam correction (Thermo Scientific ICE  
209 3400®). The standard-addition method and the addition of a constant volume of  $\text{MgNO}_3$   
210 solution (matrix modifier) were used to eliminate the matrix effects during the absorption and  
211 to allow measurements near the detection limit.  $^9\text{Be}$  sample concentrations (Table 1) were  
212 determined from repeated absorbance measurements (4 times) performed on each of the four  
213 100  $\mu\text{l}$  aliquots of the sample solution, three of them being spiked with increasing amount of a  
214 Sharlau  $^9\text{Be}$ -carrier diluted to a known concentration ( $0.27 - 0.34 \times 10^{-8} \text{ g.g}^{-1}$ ) using  $\text{HNO}_3$   
215 0.2%. The standard deviation of repeated absorbance measurements for each sample must be  
216 less than 3% to be accepted. After correcting for sample dilution, the authigenic  $^9\text{Be}$  sample  
217 concentrations along core PC16 vary around  $1.99 \pm 0.83 \cdot 10^{-7} \text{ g.g}^{-1}$ . The associated  
218 uncertainties ( $2\sigma$ ) varying from 0.4 to 3.2% (average value: 1.5%) are based on the  
219 reproducibility of measurements and the least-square fitting between measured absorbance at  
220 each stages of the standard-addition method ( $r^2 > 0.9995$ ).

221 The natural authigenic  $^{10}\text{Be}$  concentration measurements were performed at the French AMS  
222 national facility ASTER (CEREGE).  $^{10}\text{Be}$  sample concentrations are calculated from the  
223 measured spiked  $^{10}\text{Be}/^9\text{Be}$  ratios normalized to the NIST 4325 Standard Reference Material

224  $(2.79 \pm 0.03 \times 10^{-11}$ ; Nishiizumi *et al.*, 2007), and are decay-corrected using the  $^{10}\text{Be}$  half-life  
 225  $(T_{1/2})$  of  $1.387 \pm 0.012$  Ma (Chmeleff *et al.*, 2010; Korschinek *et al.*, 2010):

$$226 \quad \text{Authigenic } \left[ \frac{^{10}\text{Be}}{^9\text{Be}} \right]_{at}^{\text{decay-corrected}} = \left( \frac{^{10}\text{Be}}{^9\text{Be}} \right)_M \times \left( \left[ ^9\text{Be} \right]_{at} + m_{\text{spike}} \times \left[ ^9\text{Be} \right]_{\text{spike}} \times \frac{N_A}{M^9\text{Be}} \right) \times e^{\left( \frac{\ln(2)}{T_{1/2}} \times t \right)} \quad (1)$$

227 where:  $(^{10}\text{Be}/^9\text{Be})_M$  is the measured Be ratio;  $m_{\text{spike}}$  and  $\left[ ^9\text{Be} \right]_{\text{spike}}$  are respectively the mass  
 228 and the concentration of the added spike;  $N_A$  is the Avogadro constant ( $6.02214 \cdot 10^{23} \text{ mol}^{-1}$ );  
 229  $M^9\text{Be}$  is the beryllium Molar Mass ( $9.0121822 \text{ g} \cdot \text{mol}^{-1}$ ) and  $t$  is the time. The  $^9\text{Be}$   
 230 concentrations measured at the AAS are transformed in atoms as follow:

$$231 \quad \text{Authigenic } \left[ ^9\text{Be} \right]_{at} = \left[ ^9\text{Be} \right]_{\text{AAS}} \times m'_{\text{sample}} \times \frac{N_A}{M^9\text{Be}} \quad (2)$$

232 where:  $\left[ ^9\text{Be} \right]_{\text{AAS}}$  is the concentration of natural authigenic  $^9\text{Be}$  measured at the AAS and

$$233 \quad m'_{\text{sample}} = m_{\text{sample}} \times \left( \frac{m_{\text{leached}} - m_{\text{aliquot}}}{m_{\text{leached}}} \right) \text{ is the weight of sediment remaining after aliquot}$$

234 sampling.

235 The uncertainties ( $2\sigma$ ) in the measured  $^{10}\text{Be}/^9\text{Be}$  ratios and in the calculated  $^{10}\text{Be}$   
 236 concentrations result from statistical and instrumental error propagation (Arnold *et al.*, 2010)  
 237 and vary from 1.3 to 3.7% (average value: 2.2%).

238 The authigenic natural  $^{10}\text{Be}/^9\text{Be}$  ratios are derived using equations (1) and (2):

$$239 \quad \text{Authigenic } \left( \frac{^{10}\text{Be}}{^9\text{Be}} \right) = \frac{\left[ ^{10}\text{Be} \right]_{at}^{\text{decay-corrected}}}{\left[ ^9\text{Be} \right]_{at}} \quad (3)$$

240 The measured and calculated ratios and their uncertainties are presented in Table 1. The  
 241 uncertainties ( $2\sigma$ ) of the calculated authigenic  $^{10}\text{Be}/^9\text{Be}$  ratios are derived from the  
 242 propagation of both uncertainties and vary between 2.9 and 9% (average value: 5.5%).  
 243 Chemistry blank ratios range from  $5.3 \times 10^{-15}$  to  $1.5 \times 10^{-14}$ , which is at least 3 orders of  
 244 magnitude lower than the sample  $^{10}\text{Be}/^9\text{Be}$  ratios.

245 3.5. Measurements of  $^{230}\text{Th}_{\text{xs}}$  in Baffin Bay sediments

246 In this study, we benefit from recent U and Th-series isotope results from PC16 in order to  
247 calculate  $^{10}\text{Be}$ -fluxes ( $^{230}\text{Th}_{\text{xs}}$ -normalized). The measurements and calculation used for  
248 determining  $^{230}\text{Th}_{\text{xs}}$  are detailed in Nuttin and Hillaire-Marcel (2015). The estimated initial  
249  $^{230}\text{Th}_{\text{xs}}$  activities, recalculated in respect to the revised chronology, are extremely variable  
250 ranging from  $0.118 \pm 0.081$  to  $5.293 \pm 0.212$  dpm.g $^{-1}$  ( $1.145$  dpm.g $^{-1}$  on average with a standard  
251 deviation of  $0.977$ ). Except for few samples, large surplus of  $^{230}\text{Th}_{\text{xs}}$  above the production  
252 from dissolved-U decay in the overlying water column points toward a sediment-focusing  
253 environment related to ice margin dynamics during the last glacial period. The preserved,  
254 decay-corrected,  $^{230}\text{Th}_{\text{xs}}$ -normalized  $^{10}\text{Be}$  deposition rates (referred to  $^{10}\text{Be}$ -fluxes hereinafter)  
255 are calculated as follow:

$$256 \quad \text{Flux} [^{10}\text{Be}] = \frac{[^{10}\text{Be}]_{\text{at/g}}^{\text{decay.corrected}} \times Z \times \beta_{230}}{A_{\text{Th}-230}^{\text{xs}}} \quad (4)$$

257 where:  $[^{10}\text{Be}]^{\text{decay.corrected}}$  is the  $^{10}\text{Be}$  concentration at the time of deposition in atoms per gram  
258 of sediment;  $Z$  is the water depth (2063 m);  $\beta_{230}$  is the  $^{230}\text{Th}$  production rate from the seawater  
259  $^{234}\text{U}$  decays throughout the water column ( $2.67 \cdot 10^{-2}$  dpm.m $^{-3}$ .y $^{-1}$ ; François *et al.*, 2004) and

260  $A_{\text{Th}-230}^{\text{xs}} = A_{\text{Th}-230}^{\text{xs}} \times e^{\left(\frac{\ln(2)}{T_{1/2}} \times t\right)}$  is the scavenged  $^{230}\text{Th}_{\text{xs}}$  concentration at the time of deposition.

261 The uncertainties ( $2\sigma$ ) of the calculated  $^{10}\text{Be}$ -fluxes are derived from the propagation of both  
262 uncertainties and vary between 1.6 and 25.1% (average value: 5.0%). Note that solely 2  
263 samples have uncertainties above 10% representing probable measurement outliers. The water  
264 depth was considered constant in first approximation for the calculation. The Th analyses  
265 have been performed after total digestion of 1 g of sediment, while Be isotopes were extracted  
266 from 1 g of sediment after partial leaching (in order to avoid the extraction of matricial Be;  
267 Bourlès *et al.*, 1989). Given the difference of these two approaches, the  $^{10}\text{Be}$ -fluxes calculated  
268 here thus represent minimal values. This should be considered when comparing our results

269 against reference values, but it does not prevent any qualitative interpretations. A constant  
270 leaching efficiency of ~60 % (Bourlès *et al.*, 1989) has been verified based on the results from  
271 Ménabréaz *et al.* (2011) and Ménabréaz (2012) and can be use for calibration.

## 272 **4. Results and discussion**

273 Sample concentrations, ratios and fluxes are listed in Table 1 and presented *vs.* depth along  
274 the core photos, CT-Scan images and description in Figures 3 and 5. Sample ratios and fluxes  
275 are presented *vs.* age in Figures 7 and 8. Note that all results and statistical averages are  
276 reported hereafter with a  $\pm 2\sigma$  uncertainty.

### 277 4.1. Authigenic $^{10}\text{Be}$ and $^9\text{Be}$ concentrations

278 The authigenic  $^{10}\text{Be}$  (decay-corrected) concentrations vary from  $0.051\pm 0.002$  to  $6.403\pm 0.085$   
279  $\times 10^8 \text{ at.g}^{-1}$  (mean:  $1.64 \times 10^8 \text{ at.g}^{-1}$ ;  $\sigma=1.74$ ). Such broad variability ( $> 2$  orders of magnitude)  
280 is unusual in marine records where  $^{10}\text{Be}$  concentrations usually vary by factors of 2 or 3.  
281 Comparable large amplitude variation was only found in few polar cores from the Lomonosov  
282 Ridge (central Arctic), Fram Strait and the Ross Sea (Antarctica) where  $^{10}\text{Be}$  concentration  
283 ranging from 0.2 to  $19.5 \times 10^8 \text{ at.g}^{-1}$  (Eisenhauer *et al.*, 1994; Spielhagen *et al.*, 1997, 2004;  
284 Aldahan *et al.*, 1997; Sjunneskog *et al.*, 2007) were interpreted as paleoclimatic signals with  
285 high (resp. low)  $^{10}\text{Be}$  concentrations during Interglacial or major Interstadial (resp. Glacial)  
286 periods. Given the temporal resolution of core PC16, we can argue that in Baffin Bay the  $^{10}\text{Be}$   
287 concentration varies on shorter time scales and is not directly related to Glacial/Interglacial  
288 cycles contrary to the mechanism proposed for the Arctic Ocean. The mean  $^{10}\text{Be}$   
289 concentrations in Baffin Bay are slightly lower than values from the central Arctic and  
290 Arctic/Nordic Seas of  $3\text{-}4 \times 10^8 \text{ at.g}^{-1}$  and  $6.7 \times 10^8 \text{ at.g}^{-1}$ , respectively (Frank *et al.*, 2008;  
291 Eisenhauer *et al.*, 1994; Aldahan *et al.*, 1997), as well as with values from lower latitude sites  
292 such as the Portuguese margin and the Golf of Papua:  $\sim 4.4 \times 10^8 \text{ at.g}^{-1}$  and  $\sim 5.6 \times 10^8 \text{ at.g}^{-1}$ ,

293 respectively (Carcaillet *et al.*, 2004b; Ménabréaz *et al.*, 2011, 2014). A strict interpretation of  
294 the  $^{10}\text{Be}$  concentration in term of atmospheric fluxes between distinct sites must be avoided  
295 because of environmental parameters. However, the overall low  $^{10}\text{Be}$  concentration from  
296 Baffin Bay compared to low-latitude and Arctic sites suggests relatively reduced  $^{10}\text{Be}$  inputs  
297 to the coring site (especially within the very low  $^{10}\text{Be}$  concentration interval at 232-275 cm  
298 depth).

299 The authigenic  $^9\text{Be}$  concentrations vary from  $0.621\pm 0.004$  to  $3.269\pm 0.065 \times 10^{16}$  at.g $^{-1}$  (mean:  
300  $1.33 \times 10^{16}$  at.g $^{-1}$ ;  $\sigma=0.56$ ). The variability of  $^9\text{Be}$  concentration is about 25 times lower than the  
301  $^{10}\text{Be}$  variation. Still, this range of variation (~5 times) is larger than the variability observed in  
302 lower-latitude marine cores (~2 times), advocating for important  $^9\text{Be}$  transport and deposition  
303 changes along core PC16. The mean  $^9\text{Be}$  concentration values from PC16 are lower than  
304 those from the Portuguese margin and the Golf of Papua,  $2-4 \times 10^{16}$  at.g $^{-1}$ , but slightly higher  
305 than values from the central Arctic ( $0.6-1 \times 10^{16}$  at.g $^{-1}$ ) and from ODP983 site ( $\sim 0.25 \times 10^{16}$   
306 at.g $^{-1}$ ; Knudsen *et al.*, 2008). Notwithstanding specific interpretations related to each sites,  
307 this comparison reveals the strong association between  $^9\text{Be}$  concentration and terrigenous  
308 inputs (*e.g.*, Bourlès *et al.*, 1989; Brown *et al.*, 1992). We can argue that the central and  
309 deepest part of Baffin Bay is a sediment-focusing area that received slightly more  $^9\text{Be}$  inputs  
310 than deep open ocean basins because of its proximity to continental margins and the reduced  
311 size and shape of the bay. This is in accordance with the U-Th results from PC16 (Nuttin and  
312 Hillaire-Marcel, 2015).

313 The fluctuations of  $^{10}\text{Be}$  and  $^9\text{Be}$  concentrations present a high correlation coefficient ( $r=0.88$ ,  
314 Table 2), suggesting that sources of  $^{10}\text{Be}$  and  $^9\text{Be}$  into the bay (Figure 3) are both located on  
315 the boarding continents and that the atmospheric  $^{10}\text{Be}$  component directly precipitated over  
316 the bay likely represents minor amounts compared to these large inputs of continental origin.

#### 317 4.2. Authigenic $^{10}\text{Be}/^9\text{Be}$ ratios

318 The authigenic  $^{10}\text{Be}/^9\text{Be}$  ratios ranging from  $0.043\pm 0.003$  to  $2.624\pm 0.123 \times 10^{-8}$  (mean:  $1.01 \times$   
319  $10^{-8}$ ;  $\sigma=0.86$ ) disclose a variability over almost 2 orders of magnitude very similar to those of  
320  $^{10}\text{Be}$  and  $^9\text{Be}$  concentrations. The fact that authigenic  $^{10}\text{Be}/^9\text{Be}$  ratio values are broadly  
321 coherent with  $^{10}\text{Be}/^9\text{Be}$  ratio values ranging from 0.36 to  $1.54 \times 10^{-8}$  measured in Arctic rivers  
322 (Franck *et al.*, 2009) supports the continental origin of the dissolved beryllium in Baffin Bay.  
323 Measurements from the Baffin Bay watersheds are however required to further discuss this  
324 issue. The authigenic  $^{10}\text{Be}/^9\text{Be}$  ratio population can be divided in two groups: values (1) lower  
325 than  $10^{-8}$  and (2) higher than  $10^{-8}$  (Table 1, Figures 3, 5 and 6). The first group has  $^{10}\text{Be}$   
326 concentrations and  $^{10}\text{Be}/^9\text{Be}$  ratios similar to those found within poorly sorted diamicton  
327 layers of the Ross Ice Shelf (Sjunneskig *et al.*, 2007) and of Arctic sediments of the last 350  
328 kyr (*e.g.*, Aldahan *et al.*, 1997). They are thus coherent with other records from Polar  
329 Regions. The second group presents higher values in range with the lower limits of authigenic  
330  $^{10}\text{Be}/^9\text{Be}$  ratios from mid-to-low-latitude cores with similar sedimentation rates (Carcaillet *et*  
331 *al.*, 2004b; Ménébréaz *et al.*, 2014). This nearly bi-modal distribution of the authigenic  
332 beryllium concentrations and ratios presents a strong affinity with lithofacies changes  
333 (Figures 3 and 5).

#### 334 4.3. Beryllium and sedimentological features

335 From the authigenic Be result variations presented above, questions arise about the nature of  
336 the forcing parameters. In order to understand the links with lithofacies changes, core PC16  
337 offers a unique opportunity because of the numerous multi-proxy results available. The  
338 detailed sedimentological features of core PC16 have been largely presented and discussed  
339 elsewhere (see Simon *et al.*, 2012, 2014, in prep.; Simon, 2013; Nuttin and Hillaire-Marcel,  
340 2015 for details) and are beyond the scope of this paper. Sediment compositional variability  
341 in core PC16 is a combination of changes in sediment delivery, transport and provenance

342 directly related to ice margin dynamics (Simon *et al.*, 2014). This variability is illustrated here  
343 by grain-size (bulk and magnetic), density (CT number), XRF Ca/Fe and XRD Carbonate  
344 percents along with the images and CT-Scans of core PC16 (Figures 3 and 8) and summarized  
345 by a principal component analysis (PCA; Table S1, Figure 4) that disentangle the main  
346 compositional (mineralogy and grain-size) changes. The first principal component (PC1)  
347 accounts for 61% of the total variance and has positive loadings with proxies of coarse detrital  
348 carbonate layers such as dolomite and calcite (XRD), XRF Ca, density and >63  $\mu\text{m}$  %; and  
349 negative loadings with proxies related to finer sediments, feldspars (XRD) and XRF Fe and Ti  
350 (Figures 3 and 4; Table 2). It highlights the two main sedimentation features from Baffin Bay:  
351 *i.e.*, coarse-grained carbonate-rich sediments transported by icebergs and sea ice originating  
352 from the northern end of the bay against fine-feldspar rich sediments originating from  
353 Greenland and Baffin Island (Simon *et al.*, 2014).

354 Table 2 presents the correlation coefficients between Be isotopes and the sedimentological  
355 parameters. As suggested from Figures 3 and 7, the high correlation coefficients between PC1  
356 and Be isotopes and ratios (>-0.8) express a strong association with sedimentological  
357 parameters. The authigenic beryllium values ( $^{10}\text{Be}$ ,  $^9\text{Be}$  and  $^{10}\text{Be}/^9\text{Be}$  ratios) generally present  
358 significant increases at levels corresponding to fine grained feldspar-rich intervals associated  
359 with increases of clay minerals (30-50%; Simon *et al.*, 2014) while coarse carbonate-rich  
360 sediments (30-40% dolomite and 10-15% calcite) are characterized by lower Be values  
361 (Figure 3). This pattern is consistent with the scavenging efficiency of dissolved Be that  
362 depends on the composition and size of the particles available in the water column. The  
363 authigenic beryllium ( $^{10}\text{Be}$ ,  $^9\text{Be}$  and  $^{10}\text{Be}/^9\text{Be}$  ratios) and thorium-excess ( $^{230}\text{Th}_{\text{xs}}$ ) distribution  
364 are strongly grain size dependent, with significant positive correlations with very fine to fine  
365 silts (2-8  $\mu\text{m}$ ) while clays (0-2  $\mu\text{m}$ ) and medium to very coarse silts (8-63  $\mu\text{m}$ ) does not  
366 present any significant correlations (Table 2). The high correlation of authigenic Be isotopes



367 with the 2-8  $\mu\text{m}$  fraction rather than with the clay-sized material is intriguing because we  
368 expected larger association with the smaller particles (because of their higher specific surface  
369 area available). We tentatively explain these results by the cohesive behavior of the clay-sized  
370 material that tends to form aggregate. These aggregates would have faster sinking rates and  
371 lower specific surface area available for the adsorption of dissolve Be explaining higher  
372 scavenging rates associated with very fine to fine silts. To the opposite, the authigenic Be  
373 concentrations and ratios are significantly anti-correlated with the coarser intervals ( $>63 \mu\text{m}$ ,  
374 Figure 3) related to iceberg transported sediments (*i.e.*, BBDC). Despite an overall similar  
375 behavior of both isotopes in respect to sedimentary parameters, the authigenic  $^{10}\text{Be}$   
376 concentrations and authigenic  $^{10}\text{Be}/^9\text{Be}$  ratios are usually slightly more correlated with  
377 sedimentological parameters than  $^9\text{Be}$  isotopes. We interpret this difference by distinct  
378 sources and transport processes between both isotopes. The continental inherited- $^{10}\text{Be}$  (*i.e.*,  
379 atmospheric  $^{10}\text{Be}$  deposited onto ice-sheets) are derived from the melting and calving of ice  
380 sheets and are released in the water column during the ice melting, while the  $^9\text{Be}$  isotopes are  
381 mainly coming from the mechanical erosion of bedrocks at the basal interface of ice streams.  
382 It is likely that a fraction of the dissolved  $^9\text{Be}$  isotopes was scavenged rapidly on the  
383 continental margins within the buoyant turbid meltwater plumes or nepheloid layers (*i.e.*, re-  
384 suspension of fine sediment particles by bottom currents) due to higher particles  
385 concentration (Bacon and Rutgers van der Loeff, 1989) while the  $^{10}\text{Be}$  transported within  
386 icebergs or sea ice was exported farther from the sources. A fraction of  $^9\text{Be}$  would thus be  
387 immobilized in glacial/river estuaries (Kusakabe *et al.*, 1991) and removed from the water  
388 column within the less saline meltwater plumes on the inner-shelf (Frank *et al.*, 2009; Ó  
389 Cofaigh *et al.*, 2013) rather than being transported to the centre of the bay. Therefore, despite  
390 complex relationships between granulometry and mineralogy of these sediments, we can claim

391 that the authigenic  $^{10}\text{Be}$  signatures in Baffin Bay reveal local marine and glacial influences  
392 from the surrounding continents instead of reflecting a global  $^{10}\text{Be}$ -production signal.

#### 393 4.4. $^{10}\text{Be}$ -fluxes ( $^{230}\text{Th}_{\text{xs}}$ -normalized)

394 The preserved vertical  $^{10}\text{Be}$  deposition rates ( $^{10}\text{Be}$ -fluxes) varies from  $0.717\pm 0.046$  to  
395  $25.388\pm 0.973 \times 10^8 \text{ at.cm}^{-2}.\text{ka}^{-1}$  with a mean value of  $6.94 \times 10^8 \text{ at.cm}^{-2}.\text{ka}^{-1}$  and a standard  
396 deviation of 7.037 expressing a large variability (Table 1, Figure 5). When increased by a  
397 factor of 40%, to encompass the methodological bias induced by the partial leaching of Be  
398 isotopes vs. the total digestion of Th (see section 3.5), the  $^{10}\text{Be}$ -fluxes are oscillating between  
399  $1.004\pm 0.065$  to  $35.544\pm 1.362 \times 10^8 \text{ at.cm}^{-2}.\text{ka}^{-1}$  with an average of  $9.72 \times 10^8 \text{ at.cm}^{-2}.\text{ka}^{-1}$   
400 (Table 3). The Holocene average  $^{10}\text{Be}$ -flux is estimated at  $7.6\pm 0.2 \times 10^8 \text{ at.cm}^{-2}.\text{ka}^{-1}$  ( $10.7\pm 0.2$   
401  $\times 10^8 \text{ at.cm}^{-2}.\text{ka}^{-1}$  value corrected), while during the glacial period the fluxes oscillated around  
402  $14.3\pm 0.5$  ( $20.1\pm 0.7$ ) and  $2.0\pm 0.2$  ( $2.8\pm 0.2$ )  $\times 10^8 \text{ at.cm}^{-2}.\text{ka}^{-1}$  within the carbonate-free and  
403 carbonate-rich layers, respectively (carbonate layers are highlighted by white banding in  
404 Figures 3 and 5). The Holocene  $^{10}\text{Be}$ -fluxes are similar with the actual  $^{10}\text{Be}$  production of  
405  $12.1\pm 0.3 \times 10^8 \text{ at.cm}^{-2}.\text{ka}^{-1}$  (Monaghan *et al.*, 1986). During the glacial period, results of  $^{10}\text{Be}$ -  
406 fluxes ranging from 0.7 to  $25.4 \times 10^8 \text{ at.cm}^{-2}.\text{ka}^{-1}$  are coherent with the bulk  $^{10}\text{Be}$ -fluxes  
407 calculated in the Arctic and Fram Strait that range from  $2 \times 10^8$  to  $33 \times 10^8 \text{ at.cm}^{-2}.\text{ka}^{-1}$   
408 (Eisenhauer *et al.*; 1994; Aldahan *et al.*, 1997). Despite an obvious sedimentological  
409 relationship in core PC16, and at the exception of few intervals, the  $^{10}\text{Be}$ -fluxes are  
410 compatible with the modeled  $^{10}\text{Be}$ -production range:  $\sim 3$  to  $27 \times 10^8 \text{ at.cm}^{-2}.\text{ka}^{-1}$ ; with the  
411  $^{10}\text{Be}$ -fluxes from ice and marine records which range from  $\sim 1.2$  to  $70 \times 10^8 \text{ at.cm}^{-2}.\text{ka}^{-1}$ , and  
412 with the globally integrated and long-term averaged  $^{10}\text{Be}$ -fluxes into marine sediments  
413 varying between 9 to  $28 \times 10^8 \text{ at.cm}^{-2}.\text{ka}^{-1}$  (see Table 3 for details and references). The lowest  
414  $^{10}\text{Be}$ -fluxes that characterized the BBDC layers are also rather similar to those found within  
415 the Ice Summit record of GISP2:  $2$  to  $6 \times 10^8 \text{ at.cm}^{-2}.\text{ka}^{-1}$  (Muscheler *et al.*, 2004). It is

416 puzzling to obtain  $^{10}\text{Be}$ -fluxes similar to ice core records in core PC16 given the strong  
417 lithogenic imprint. This similarity might be explained by a smoothing of the  $^{10}\text{Be}$  cosmogenic  
418 nuclide signal related to the long-lasting deposition/drift onto the regional ice-sheets and by  
419 the thick sea ice and/or ice-shelf cover during glacial periods. The relatively low  $^{10}\text{Be}$ -fluxes  
420 calculated in Baffin Bay would thus likely represent a  $^{10}\text{Be}$  production signal buffered by the  
421 glacial factors controlling the  $^{10}\text{Be}$  inputs and transport within the water column. Furthermore,  
422 these low  $^{10}\text{Be}$ -fluxes from Baffin Bay are also coherent with the low depositions of  $^{10}\text{Be}$  in  
423 Greenland and in the Arctic Ocean (Eisenhauer *et al.*, 1994; Spielhagen *et al.*, 1997) likely  
424 due to atmospheric circulation patterns and the distribution of precipitation in the northern  
425 hemisphere (Heikkila *et al.*, 2013; Frank *et al.*, 2009).

#### 426 4.5. Testing the $^{10}\text{Be}/^9\text{Be}$ ratios and $^{230}\text{Th}_{\text{xs}}$ -normalized $^{10}\text{Be}$ fluxes methods

427 The two existing normalization methods were independently used in former studies, but only  
428 two studies applied the two methods on the same sedimentary core. The first study by  
429 Knudsen *et al.* (2008) obtained large uncertainties about  $^{230}\text{Th}_{\text{xs}}$  values precluding their use  
430 for reliable normalization. The second study by Ménabréaz *et al.* (2011) demonstrated close  
431 agreement of the results obtained by the two methods based on a small number of samples. In  
432 PC16, the  $^{10}\text{Be}$ -flux variability calculated using the  $^{230}\text{Th}_{\text{xs}}$  method is similar to that of the  
433 authigenic  $^{10}\text{Be}/^9\text{Be}$  ratios measured at the same depths (Figure 5). The high correlation  
434 coefficient ( $r=0.81$ ) and coherence between the two signals provide strong evidence that the  
435 two normalization processes yield equivalent results in a very contrasted environment where  
436 large compositional variations prevailed (Figures 5 and 6, Table 2). It somehow demonstrates  
437 that normalizing authigenic  $^{10}\text{Be}$  concentrations by authigenic  $^9\text{Be}$  concentrations permits an  
438 accurate correction for the total particle flux variation. Both normalization processes present  
439 large variations directly related to lithofacies changes (Figure 3). The normalizers (*i.e.*,  $^{230}\text{Th}_{\text{xs}}$   
440 and  $^9\text{Be}$ ) are highly correlated (Table 2) which might seem surprising given the distinct

441 affinities (depending on particle composition) and the different scavenging residence times of  
442 both elements in the open ocean (10-50 years for Th against 500-1000 years for Be, Chase *et*  
443 *al.*, 2002). The large domination of glaciomarine lithogenic particles presenting strong surface  
444 reactivity with both nuclides probably explained the first assertion (Roy-Barman *et al.*, 2005,  
445 2009). Our results also suggest quicker adsorption rates and thus shorter scavenging residence  
446 time for dissolved Be within the Baffin Bay water column probably related to the high  
447 concentration of lithogenic particles. This is coherent with previous results from the Arctic,  
448 North Atlantic basin and circum-Antarctica where lower scavenging residence time for Be  
449 isotopes of about 80-200 years associated with high particles concentration and oceanic  
450 mixing have been proposed (von Blanckenburg *et al.*, 1996, 1999; von Blanckenburg and  
451 Bouchez, 2014; Frank *et al.*, 2009). An oceanic circulation/mixing influence over the  
452 authigenic Be signal into Baffin Bay during the glacial period is also supported by higher  
453 correlation coefficients between both normalization methods when considering the rare  
454 episodes of Arctic Waters overflow through the Davis Strait (illustrated by blue dots in  
455 Figures 5 and 6). These episodes have been demonstrated within core PC16 by the occurrence  
456 of short periods of  $^{230}\text{Th}_{\text{xs}}$  export ( $^{230}\text{Th}_{\text{xs}}$ -losses, Nuttin and Hillaire-Marcel, 2015).

#### 457 4.6. Comparison with relative paleointensity

458 In core PC16, the comparison of  $^{10}\text{Be}$ -proxies with the RPI record does not demonstrate any  
459 clear relationship (Figure 7). No systematic increases of authigenic  $^{10}\text{Be}/^9\text{Be}$  ratios and  $^{10}\text{Be}$ -  
460 fluxes are observed during the large RPI lows corresponding to the Laschamp, Norwegian-  
461 Greenland Sea and post-Blake/Blake events (Figure 7). The authigenic  $^{10}\text{Be}/^9\text{Be}$  ratios and  
462  $^{10}\text{Be}$ -fluxes do not present any significant correlation coefficients with the RPI record (Figure  
463 7, Table 2). This absence of correlation with the RPI record clearly supports the dominance of  
464 the environmental imprints –as discussed above- on the  $^{10}\text{Be}$  deposition in Baffin Bay. The  
465 high correlation ( $r=0.83$ ) between the RPI normalizers (such as the ARM) and the authigenic

466  $^{10}\text{Be}/^9\text{Be}$  ratios also indicates a strong environmental imprint related to specific grain-size  
467 ranges that insure maximum Be adsorption rates (namely the very fine to fine silt range is  
468 highly correlated with the ARM:  $r=0.7$ ). The strong correlation of the  $^{10}\text{Be}$ -proxies with  
469 environmental parameters suggests a local signature related with the succession of events  
470 driven by paleoclimatic controls precluding any interpretation of the  $^{10}\text{Be}$ -proxies in term of  
471 geomagnetic variability. On the opposite, our findings provide strong evidence supporting the  
472 use of the cosmogenic nuclide  $^{10}\text{Be}$  as a stratigraphic marker in the Arctic and sub-Arctic  
473 regions as suggested by several authors (Eisenhauer *et al.*, 1994; Spielhagen *et al.*, 1997;  
474 Aldahan *et al.*, 1997; Frank *et al.*, 2008).

## 475 **5. Paleoenvironmental implications**

476 The quasi bi-modal distribution of Be results in core PC16 corresponding with the main  
477 Baffin Bay sedimentary features (Figure 3) and the temporal resolution of Be variations  
478 suggest glacial dynamics as the main forcing parameter to explain Be inputs and transport  
479 changes. The most striking features of this glacial dynamic around Baffin Bay is the  
480 variability of the GIS limits over the Greenland continental shelf and the ice streaming events  
481 from the LIS and IIS together with sea ice/ice-shelf cover variability (Figure 9). The origin,  
482 timing and limits of these large glacial variations are still very poorly constrained. However,  
483 recent studies have demonstrated that ice-sheets advanced well onto the continental margins  
484 all over the bay and as far as the shelf edges during the LGM (Li *et al.*, 2011; Ó Cofaigh *et*  
485 *al.*, 2012, 2013; Hogan *et al.*, 2012; Dowdeswell *et al.*, 2013; Simon *et al.*, 2014; Margold *et*  
486 *al.*, 2015).

487 The cumulative inventory of measured  $^{230}\text{Th}_{\text{xs}}$  in core PC16 (see Nuttin and Hillaire-Marcel,  
488 2015 for details), recalculated in respect to the revised age model, clearly exhibits maximal  
489 sediment fluxes corresponding to minimum relative sea level (RSL) during the LGM (Figure  
490 8). High Be concentrations (Figures 7 and 8) and *ca.* 100% sediments originating from

491 Greenland (Simon *et al.*, 2014) also characterized this period. The other periods of high  
492 authigenic Be concentrations are also associated with finer sediments originating mainly from  
493 Greenland (Figure 8). This facies is related to the resuspension of fine lithogenic sediments  
494 (glacial flour) associated to nepheloid layers during period of intense ice margin advances, to  
495 outflow of dense winter water from the continental shelves, or to meltwater sediment-laden  
496 plumes during period of ice margin retreats. Both scenarios imply ice margins/ice streams  
497 extending over the Greenland continental shelf. Together with the inherent higher scavenging  
498 efficiency of smaller particles, the increase in particle concentration due to the proximal ice  
499 margin likely contributed to the increase of the Be-scavenging rates in central Baffin Bay  
500 (Figure 9). We can also assume that a fraction of the Be transported onto ice floes sediments  
501 might be transferred into the water column by wave wash-off or turning of floes during these  
502 glacial maxima. Two  $^{10}\text{Be}$  concentration values of  $2.2\pm 0.1$  and  $2.8\pm 0.1 \times 10^8 \text{ at.g}^{-1}$  measured  
503 in clay samples from Arctic ice floes (Eisenhauer *et al.*, 1994) and corresponding to the  
504 higher  $^{10}\text{Be}$  concentration values from PC16 support this assumption, although samples from  
505 Baffin Bay are requested to further discuss this assertion.

506 On the other hand, the low authigenic Be concentrations and ratios within the BBDC layers  
507 support a Be dilution in these IRD layers (Figure 2). Such a dilution is possibly associated to  
508 (1) increases of terrigenous sediment inputs, (2) changes of sediment composition/grain-size  
509 affecting the scavenging efficiency of dissolved beryllium, (3) reduced net Be inputs into the  
510 centre of the bay and/or (4) higher exports of Be by extensive sea ice/iceberg drift episodes.  
511 The absence of significant increases in sedimentation rates (Figure 8) and/or  $^{230}\text{Th}_{\text{xs}}$  changes  
512 (Nuttin and Hillaire-Marcel, 2015) during these intervals favor the last three hypotheses.  
513 However one cannot totally exclude that short episodes of increased inputs of terrigenous  
514 sediments could remain uncaptured by the age model resolution. During the BBDC intervals,  
515 the limited amount of sediment originating from Greenland supports a distant Greenland ice

516 margin limit while coarse sediments originating from Baffin Island are explained by high  
517 calving rates from Laurentide ice streams (Simon *et al.*, 2014). According to this model, the  
518 BBDC intervals occur during periods of retreated ice limits over the inner continental shelves  
519 (Figure 9). The cause of ice margin instabilities around Baffin Bay is still not well understood  
520 but may be related to higher summer insolation and/or to the advection of warm Atlantic  
521 Water. Indeed the phasing between magnetic grain size in core PC16 (SIRM/ $k_{LF}$  ratios in  
522 Figure 8, Simon *et al.*, 2012, 2014) and the insolation variation supports a climatic control on  
523 ice margin dynamics and iceberg drifting in the bay. The advection of an intermediate warm  
524 water mass in Baffin Bay probably contributed also to destabilize the ice margins (Holland *et*  
525 *al.*, 2008; Jennings *et al.*, 2014) increasing meltwater delivery along the Baffin Bay shelves  
526 and slopes. It resulted in increased stratification of the water column and therefore to longer  
527 residence times of Be within the deep water masses (von Blanckenburg and O'Nions, 1999).  
528 Such an oceanic pattern would reduce the Be adsorption and deposition rates explaining  
529 possibly part of the low  $^{10}\text{Be}$  concentration within the BBDC intervals. Moreover, and despite  
530 complex interactions of eustatic and isostatic parameters over the relative sea level (RSL)  
531 around Baffin Bay, we can reasonably assess that the sea level rose over continental shelves  
532 during ice margin retreat periods (Long *et al.*, 2008; Simpson *et al.*, 2009; Funder *et al.*,  
533 2011). Throughout these periods of marine transgression, oceanic circulation and boundary  
534 scavenging (changes in nature and intensity, Lao *et al.* 1992) may have become significant  
535 processes involving large transfer of dissolved Be from the centre of the bay toward the  
536 margins (Roy-Barman *et al.*, 2009). The low authigenic  $^{10}\text{Be}/^9\text{Be}$  ratios and  $^{10}\text{Be}$ -fluxes  
537 during the BBDC intervals within core PC16 might thus be partly explained by high boundary  
538 scavenging rates over the large Greenland continental shelf together with important  
539 iceberg/sea ice drifts due to very active Laurentide ice streams. For instance, the very low  
540 authigenic  $^{10}\text{Be}/^9\text{Be}$  ratios found during the late MIS-3 (*ca.* 40-28.5 ka BP) is explained by

541 retreated GIS limits and numerous ice streaming episodes from the LIS and IIS possibly  
542 related to the Dansgaard-Oeschger events between the large glacial surges of Heinrich-events  
543 3 and 4 (Figure 8; Simon et al., 2014).  
544 Even though interpretations resulting from the authigenic Be signature in Baffin Bay can be  
545 discussed and are likely the results of several processes, we can reasonably proposed that the  
546 glacial dynamic of regional ice sheets (*i.e.*, GIS, IIS and LIS) is the main internal driving  
547 mechanism in term of  $^{10}\text{Be}$  inputs and delivery into the bay. Moreover, ice-sheets topography  
548 changes related to such glacial dynamic also imply a reorganization of the atmospheric  
549 circulation (*e.g.*, Steffensen *et al.*, 2008) modifying the stratosphere/troposphere exchanges,  
550 the wet/dry deposition ratio and the dust inputs into the ocean (Werner *et al.*, 2002). Periods  
551 of ice-sheet growth (resp. decay) characterized by higher (resp. lower) wet deposition would  
552 then favor higher (resp. lower)  $^{10}\text{Be}$  deposition rates within the bay. Although our results are  
553 coherent with these views, atmospheric modeling of  $^{10}\text{Be}$  deposition considering regional ice-  
554 sheet topography changes are needed to verify and quantify these assumptions.

## 555 **6. Conclusions**

556 The authigenic  $^{10}\text{Be}$  cosmogenic nuclide and  $^9\text{Be}$  stable isotope data were measured along a  
557 7.41 m sedimentary core of the sub-arctic basin Baffin Bay in order to reconstruct the  
558 geomagnetic dipole moment variations using the  $^{10}\text{Be}/^9\text{Be}$  ratios and  $^{10}\text{Be}$ -fluxes ( $^{230}\text{Th}_{\text{xs}}$ -  
559 normalized). The results of the two normalizations are coherent and reveal that environmental  
560 processes such as glacial dynamics and oceanic variability directly control the variations of  
561 the authigenic  $^{10}\text{Be}$  and  $^9\text{Be}$  concentrations in Baffin Bay sediments. The contribution of the  
562 atmospheric  $^{10}\text{Be}$  cosmogenic nuclide production modulated by the geomagnetic field  
563 intensity remains hidden behind this environmental signal. Accordingly, in such conditions  
564  $^{10}\text{Be}$  production proxies do not allow to characterize the geomagnetic features such as dipole  
565 lows linked to excursions or reversals. Beryllium isotopes are preferentially adsorbed on fine



566 silicate particles associated with sediment plumes originating from lateral ice margin  
567 advances. On the contrary they have little affinity with coarse-grained and carbonate-rich  
568 sediments (*i.e.*, BBDC) associated with iceberg and sea-ice transport originated from the  
569 North-Eastern Laurentide Ice Sheet and Innuitian Ice Sheet ice streaming events. During  
570 these BBDC episodes, glacial margin retreats together with marine transgression over the  
571 Greenland continental shelf likely contributed to increase boundary scavenging involving  
572 large transfers of dissolved beryllium from the centre of the bay toward the margins. Our  
573 findings provide strong evidences that support the use of cosmogenic nuclide  $^{10}\text{Be}$  as a  
574 stratigraphic marker in the Arctic and sub-Arctic regions. Yet, our results caution a  
575 straightforward use of  $^{10}\text{Be}$ -concentrations as a proxy of Interglacial/Glacial cycles or major  
576 Interstadial periods (as suggested by several authors), and rather propose to relate the  $^{10}\text{Be}$   
577 variations to higher-frequency paleoclimatic changes and glacial dynamics. Therefore,  
578 studying the cosmogenic  $^{10}\text{Be}$  and stable  $^9\text{Be}$  isotopes in combination with ancillary  
579 sedimentological parameters in arctic and sub-arctic marine sediments provide valuable  
580 climatic information, but it must be acknowledged that the cost/information ratio is probably  
581 too large to systematically use atmospheric  $^{10}\text{Be}$  cosmogenic nuclides and  $^9\text{Be}$  isotopes as  
582 paleoclimatic proxies.

### 583 **Acknowledgements**

584 We acknowledge Valery Guillou (CEREGE) for his help during chemical sample preparation  
585 and  $^9\text{Be}$  measurements at the AAS. M. Arnold, G. Aumaître and K. Keddadouche are thanked  
586 for their valuable assistance during the measurements performed at the ASTER AMS national  
587 facility (CEREGE, Aix en Provence). This equipment is supported by the INSU/CNRS, the  
588 IRD and the CEAEA and by the ANR through the program “EQUIPEX Investissement  
589 d’Avenir”. This study is a contribution of the project MAGORB ANR 09 BLAN 0053  
590 (CEREGE, IPGP, LSCE). G. St-Onge and C. Hillaire-Marcel acknowledge financial support

591 from the Natural Science and Engineering Council of Canada (NSERC). CEREGE belongs to  
592 Observatoire des Sciences de l'Univers OSU-Institut Pythéas.

## 593 **References**

- 594 Aksu, A.E., 1985. Climatic and oceanographic changes over the past 400,000 years: evidence  
595 from deep-sea cores on Baffin Bay and Davis strait. In *Quaternary Environments:*  
596 *Eastern Canadian Arctic, Baffin Bay and Western Greenland*, Andrews JT (ed.). Allen  
597 and Unwin: Boston; 181–209.
- 598 Aksu, A.E., Piper, D.J.W., 1987. Late Quaternary Sedimentation in Baffin Bay. *Canadian*  
599 *Journal of Earth Sciences* 24 (9): 1833–46.
- 600 Aldahan, A.A., Ning, S., Possnert, G., Backman, J., Boström, K., 1997.  $^{10}\text{Be}$  records from  
601 sediments of the Arctic Ocean covering the past 350 ka. *Marine Geology* 144 (1-3):  
602 147-162.
- 603 Aldahan, A., Possnert, G., Johnsen, S., Clausen, H.B., Isaksson, E., Karlen, W., Hansson, M.,  
604 1998. Sixty year  $^{10}\text{Be}$  record from Greenland and Antarctica. *Proceedings of the*  
605 *Indian Academy of Sciences - Earth and Planetary Sciences* 107 (2): 139–147.
- 606 Alexanderson, H., Backman, J., Cronin, T.M., Funder, S., Ingólfsson, Ó., Jakobsson, M.,  
607 Landvik, J.Y., Löwemark, L., Mangerud, J., März, C., Möller, P., O'Regan, M.,  
608 Spielhagen, R.F., 2014. An Arctic perspective on dating Mid-Late Pleistocene  
609 environmental history. *Quaternary Science Reviews* 92: 9-31.
- 610 Alley, R.B., Andrews, J.T., Brigham-Grette, J., Clarke, G.K.C., Cuffey, K.M., Fitzpatrick,  
611 J.J., Funder, S., Marshall, S.J., Miller, G.H., Mitrovica, J.X., 2010. History of the  
612 Greenland Ice Sheet: Paleoclimatic insights. *Quaternary Science Reviews* 29 (15–16):  
613 1728-1756.
- 614 Andrews, J.T., Kirby, M.E., Aksu, A.E., Barber, D.C., Meese, D., 1998. Late Quaternary  
615 Detrital Carbonate (DC-) Layers in Baffin Bay Marine Sediments (67°–74° N):  
616 Correlation with Heinrich Events in the North Atlantic?. *Quaternary Science Reviews*  
617 17: 1125-1137.
- 618 Andrews, J.T., Gibb, O.T., Jennings, A.E., Simon, Q., 2014. Variations in the provenance of  
619 sediment from ice sheets surrounding Baffin Bay during MIS 2 and 3 and export to the  
620 Labrador Shelf Sea: Site HU2008029-0008 Davis Strait. *Journal of Quaternary*  
621 *Science* 29 (1): 3-13, doi:10.1002/jqs.2643.
- 622 Arnold, M., Silke, M., Boursès, D.L., Braucher, R., Benedetti, L., Finkel, R.C., Aumaître, G.,  
623 Gottang, A., Klein, M., 2010. The French accelerator mass spectrometry facility  
624 ASTER: Improved performance and developments. *Nuclear Instruments and Methods*  
625 *in Physics Research B* 268: 1954–1959, doi:10.1016/j.nimb.2010.02.107.
- 626 Auer, M., Wagenbach, D., Wild, E.M., Wallner, A., Priller, A., Miller, H., Schlosser, C.,  
627 Kutschera, W., 2009. Cosmogenic  $^{26}\text{Al}$  in the atmosphere and the prospect of a  
628  $^{26}\text{Al}/^{10}\text{Be}$  chronometer to date old ice. *Earth and Planetary Science Letters* 287: 453–  
629 462.
- 630 Bacon, M.P., 1984. Glacial to interglacial changes in carbonate and clay sedimentation in the  
631 Atlantic Ocean estimated from  $^{230}\text{Th}$  measurements. *Chemical Geology* 46 (2): 97-  
632 111.

- 633 Bacon, M.P., Rutgers van der Loeff, M.M., 1989. Removal of thorium-234 by scavenging in  
634 the bottom nepheloid layer of the ocean. *Earth and Planetary Science Letters* 92 (2):  
635 157-164.
- 636 Barker, S., Knorr, G., Edwards, R.L., Parrenin, F., Putnam, A.E., Skinner, L.C., Wolff, E.,  
637 Ziegler, M., 2011. 800,000 Years of Abrupt Climate Variability. *Science* 334 (6054):  
638 347-351, doi:10.1126/science.1203580.
- 639 Baroni, M., Bard, E., Petit, J.R., Magand, O., Bourlès D.L., 2011. Volcanic and solar activity,  
640 and atmospheric circulation influences on cosmogenic  $^{10}\text{Be}$  fallout at Vostok and  
641 Concordia (Antarctica) over the last 60 years. *Geochimica et Cosmochimica Acta* 75  
642 (22): 7132-7145, doi:10.1016/j.gca.2011.09.002.
- 643 Beer, J., Blinov, A., Bonani, G., Finkel, R.C., Hofmann, H.J., Lehmann, B., Oeschger, H.,  
644 Sigg, A., Schwander, J., Staffelbach, T., Stauffer, B., Sutter, M., Wölfli, W., 1990.  
645 Use of  $^{10}\text{Be}$  in Polar Ice to Trace the 11-Year Cycle of Solar Activity. *Nature* 347  
646 (6289): 164–166, doi:10.1038/347164a0.
- 647 Beer, J., Finkel, R.C., Bonani, G., Gäggeler, H., Glach, U., Jacob, P., Klockow, D., Langway,  
648 C.C.J., Neftel, A., Oeschger, H., Schotterer, U., Schwander, J., Siegenthaler, U., Suter,  
649 M., Wagenbach, D., Wölfli, W., 1991. Seasonal variations in the concentrations of  
650  $^{10}\text{Be}$ ,  $\text{Cl}^-$ ,  $\text{NO}_3^-$ ,  $\text{SO}_4^{2-}$ ,  $\text{H}_2\text{O}_2$ ,  $^{210}\text{Pb}$ ,  $^3\text{H}$ , mineral dust, and  $\delta^{18}\text{O}$  in Greenland snow.  
651 *Atmospheric Environment* 25 (19): 899 – 904.
- 652 Bourlès, D.L., Raisbeck, G.M., Yiou, F., 1989.  $^{10}\text{Be}$  and  $^9\text{Be}$  in Marine sediments and their  
653 potential for dating. *Geochimica et Cosmochimica Acta* 53 (2): 443–452.
- 654 Brown, E.T., Measures, C.I., Edmond, J.M., Bourlès, D.L., Raisbeck, G.M., Yiou, F., 1992.  
655 Continental inputs of beryllium to the oceans. *Earth and Planetary Science Letters* 114  
656 (1): 101-111.
- 657 Campbell D.C., de Vernal A., 2009. CCGS Hudson Expedition 2008029: Marine geology and  
658 paleoceanography of Baffin Bay and adjacent areas, Nain, NL to Halifax, NS, August  
659 28- September 23. Geological Survey of Canada, Open File 5989, 1 DVD.
- 660 Carcaillet, J.T., Thouveny, N., Bourlès, D.L., 2003. Geomagnetic moment instability between  
661 0.6 and 1.3 Ma from cosmonuclide evidence. *Geophysical Research Letters* 30 (15):  
662 1792, doi:10.1029/2003GL017550.
- 663 Carcaillet, J.T., Bourlès, D.L., Thouveny, N., 2004a. Geomagnetic dipole moment and  $^{10}\text{Be}$   
664 production rate intercalibration from authigenic  $^{10}\text{Be}/^9\text{Be}$  for the last 1.3 Ma.  
665 *Geochemistry Geophysics Geosystems* 5 (5): Q05006, doi:10.1029/2003GC000641.
- 666 Carcaillet, J.T., Bourlès, D.L., Thouveny, N., Arnold, M. 2004b. A high resolution authigenic  
667  $^{10}\text{Be}/^9\text{Be}$  record of geomagnetic moment variations over the last 300 ka from  
668 sedimentary cores of the Portuguese margin. *Earth and Planetary Science Letters* 219  
669 (3): 397–412, doi:10.1016/S0012821X03007027.
- 670 Cauquoin, A., 2013. Flux de  $^{10}\text{Be}$  en Antarctique durant les 800,000 dernières années et  
671 interpretation. PhD Thesis, Université Paris-Sud XI, pp. 206.
- 672 Cauquoin, A., Raisbeck, G.M., Jouzel, J., Bard, E., ASTER Team, 2014. No evidence for  
673 planetary influence on solar activity 330,000 years ago. *Astronomy and Astrophysics*  
674 561: A132, doi:10.1051/0004-6361/201322879.
- 675 Channell, J.E.T., Xuan, C., Hodell, D.A., 2009. Stacking paleointensity and oxygen isotope  
676 data for the last 1.5 Myr (PISO-1500). *Earth and Planetary Science Letters* 283 (1-4):  
677 14-23, doi:10.1016/j.epsl.2009.03.012.

- 678 Channell, J.E.T, Hodell, D.A., Curtis, J.H., 2012. ODP Site 1063 (Bermuda Rise) revisited:  
679 oxygen isotopes, excursions and paleointensity in the Brunhes Chron. *Geochemistry*  
680 *Geophysics Geosystems* 13 (1): Q02001, doi:10.1029/2011GC003897.
- 681 Chase, Z., Anderson, R.F., Fleisher, M.Q., Kubik, P.W., 2002. The influence of particle  
682 composition and particle flux on scavenging of Th, Pa and Be in the ocean. *Earth and*  
683 *Planetary Science Letters* 204 (1): 215-229.
- 684 Chmeleff, J., von Blanckenburg, F., Kossert, K., Jakob, D., 2010. Determination of the  $^{10}\text{Be}$   
685 half-life by multicollector ICP-MS and liquid scintillation counting. *Nuclear*  
686 *instruments and methods in physics research B.* 268 (2): 192-199,  
687 doi:10.1016/j.nimb.2009.09.012.
- 688 Christl, M., Strobl, C., Mangini, A., 2003. Beryllium-10 in deep-sea sediments: a tracer for  
689 the Earth's magnetic field intensity during the last 200,000 years. *Quaternary Science*  
690 *Reviews* 22 (5-7): 725-739, doi:10.1016/S0277-3791(02)00195-6
- 691 Christl, M., Mangini, A. Kubik, P.W., 2007. Highly resolved beryllium-10 record from ODP  
692 Site 1089 - a global signal?. *Earth and Planetary Science Letters* 257 (1-2): 245-258,  
693 doi:10.1016/j.epsl.2007.02.035.
- 694 Christl, M., Lippold, J., Steinhilber, F., Bernsdorff, F., Mangini, A., 2010. Reconstruction of  
695 global  $^{10}\text{Be}$  production over the past 250 ka from highly accumulating Atlantic drift  
696 sediments. *Quaternary Science Reviews.*" *Quaternary Science Reviews* 29 (19-20):  
697 2663-2672, doi:10.1016/j.quascirev.2010.06.017.
- 698 Cooke, D.J., Humble, J.E., Shea, M.A., Smart, D.F., Lund, N., Rasmussen, I.L, Byrnek, B.,  
699 Goret, P., Petrou, N., 1991. On cosmic-ray cut-off terminology. *Il Nuovo Cimento*  
700 14C (3): 213-234.
- 701 de Vernal, A., Hillaire-Marcel, C., Aksu, A.E., Mudie, P.J., 1987. Palynostratigraphy and  
702 chronostratigraphy of Baffin Bay deep sea cores: climatostratigraphic implications.  
703 *Palaeogeography, Palaeoclimatology, Palaeoecology* 61: 97-105.
- 704 Dowdeswell, J.A., Hogan, K.A., Ó Cofaigh, C., Fugelli, E.M.G., Evans, J., Noormets, R.,  
705 2013. Late Quaternary ice flow in a West Greenland fjord and cross-shelf trough  
706 system: submarine landforms from Rink Isbrae to Uummannaq shelf and slope.  
707 *Quaternary Science Reviews* 92: 292-309, doi:10.1016/j.quascirev.2013.09.007.
- 708 Dunai, T.J., Lifton, N.A., 2014. The Nuts and Bolts of Cosmogenic Nuclide Production.  
709 *Elements* 10 (5): 347-350. doi:10.2113/gselements.10.5.347.
- 710 Dyke, A.S., 2004. An outline of North American Deglaciation with emphasis on central and  
711 Northern Canada. *Developments in Quaternary Science* 2: 373-424.
- 712 Eisenhauer, A., Spielhagen, R.F., Frank, M., Hentzschel, G., Mangini, A., Kubik, P.W.,  
713 Dittrich-Hannen, B., Billen, T., 1994.  $^{10}\text{Be}$  records of sediment cores from high  
714 northern latitudes: Implications for environmental and climatic changes. *Earth and*  
715 *Planetary Science Letters* 124 (1): 171-184.
- 716 England, J.H., Atkinson, N., Bednarski, J., Dyke, A.S., Hodgson, D.A., Ó Cofaigh, C., 2006.  
717 The Inuitian Ice Sheet: configuration, dynamics and chronology. *Quaternary Science*  
718 *Reviews* 25 (7-8): 689-703, doi:10.1016/j.quascirev.2005.08.007.
- 719 Finkel, R.C., Nishiizumi, K., 1997. Beryllium 10 concentrations in the Greenland Ice Sheet  
720 Project 2 ice core from 3-40 ka, *Journal of Geophysical Research* 102 (C12): 26699-  
721 26706, doi:10.1029/97JC01282.

- 722 Francois, R., Frank, M., van der Loeff, R., Michiel, M., Bacon, M.P., 2004.  $^{230}\text{Th}$   
723 normalization: an essential tool for interpreting sedimentary fluxes during the late  
724 Quaternary. *Paleoceanography* 19: PA1018, doi:doi:10.1029/2003PA000939.
- 725 Frank, M., Schwarz, B., Baumann, S., Kubik, P.W., Suter, M., Mangini, A., 1997. A 200 kyr  
726 record of cosmogenic radionuclide production rate and geomagnetic field intensity  
727 from  $^{10}\text{Be}$  in globally stacked deep-sea sediments. *Earth and Planetary Science Letters*  
728 149 (1-4): 121-129.
- 729 Frank, M., 2000. Comparison of cosmogenic radionuclide production and geomagnetic field  
730 intensity over the last 200,000 years. *Philosophical Transactions of the Royal Society*  
731 *London A* 358: 1089-1107, doi: 10.1098/rsta.2000.0575.
- 732 Frank, M., Backman, J., Jakobsson, M., Moran, K., O'Regan, M., King, J., Haley, B.A.,  
733 Kubik, P.W., Garbe-Schönberg, D., 2008. Beryllium isotopes in central Arctic Ocean  
734 sediments over the past 12.3 million years: stratigraphic and paleoclimatic  
735 implications. *Paleoceanography* 23 (1): PA1S02, doi:10.1029/2007PA001478.
- 736 Frank, M., Porcelli, D., Andersson, P., Baskaran, M., Björk, G., Kubik, P.W., Hattendorf, B.,  
737 Guenther, D., 2009. The dissolved beryllium isotope composition of the Arctic Ocean.  
738 *Geochimica et Cosmochimica Acta* 73 (20): 6114–6133,  
739 doi:10.1016/j.gca.2009.07.010.
- 740 Funder S., Kjellerup K.K., Kjær K.H., Ó Cofaigh, C., 2011. The Greenland Ice Sheet during  
741 the past 300,000 Years: a review, In: Ehlers, J., Gibbard, P.L., Hughes, P.D., Editor(s),  
742 *Developments in Quaternary Sciences* (15): 699-713.
- 743 Grant, K.M., Rohling, E.J., Bar-Matthews, M., Ayalon, A., Medina-Elizalde, M., Bronk  
744 Ramsey, C., Satow, C., Roberts, A.P., 2012. Rapid coupling between ice volume and  
745 polar temperature over the past 150,000 years. *Nature* 491: 744-747,  
746 doi:10.1038/nature11593.
- 747 Heikkilä, U., Beer, J., Jouzel, J., Feichter, J., Kubik, P., 2008.  $^{10}\text{Be}$  measured in a GRIP snow  
748 pit and modeled using the ECHAM5-HAM general circulation model. *Geophysical*  
749 *Research Letters* 35: L05817, doi:10.1029/2007GL033067
- 750 Heikkilä, U., Beer, J., Feichter, J., 2009. Meridional transport and deposition of atmospheric  
751  $^{10}\text{Be}$ . *Atmospheric Chemistry and Physics* 9: 515–527.
- 752 Heikkilä, U., Beer, J., Abreu, J.A., Steinhilber, F., 2013. On the atmospheric transport and  
753 deposition of the cosmogenic radionuclides ( $^{10}\text{Be}$ ): a review. *Space Science Reviews*  
754 176 (1-4): 321-332, doi:10.1007/s11214-011-9838-0.
- 755 Hemming, S.R., 2004. Heinrich events: massive late Pleistocene detritus layers of the North  
756 Atlantic and their global climate imprint. *Reviews of Geophysics* 42 (1): RG1005,  
757 doi:10.1029/2003RG000128.
- 758 Henken-Mellies, W.U., Beer, J., Heller, F., Hsü, K.J., Shen, C., Bonami, G., Hofmann, H.J.,  
759 Suter, M., Wölfli, W., 1990.  $^{10}\text{Be}$  and  $^9\text{Be}$  in South Atlantic DSDP Site 519: relation  
760 to geomagnetic reversals and to sediment composition. *Earth and Planetary Science*  
761 *Letters* 98: 267-276.
- 762 Hillaire-Marcel, C., de Vernal, A., Aksu, A.E., Macko, S., 1989. High-resolution isotopic and  
763 micropaleontological studies of upper Pleistocene sediment at ODP site 645, Baffin  
764 Bay. *Proceedings of the Ocean Drilling Program, Scientific Results* 105: 599–616,  
765 doi:10.2973/odp.proc.sr.105.138.1989.

- 766 Hogan, K.A., Dowdeswell, J.A., Ó Cofaigh, C., 2012. Glacimarine sedimentary processes and  
767 depositional environments in an embayment fed by West Greenland ice streams.  
768 *Marine Geology* 311-314:1-16, doi:10.1016/j.margeo.2012.04.006.
- 769 Holland, D.M., Thomas, R.H., de Young, B., Ribergaard, M.H., Lyberth, B., 2008.  
770 Acceleration of Jakobshavn Isbrae triggered by warm subsurface ocean waters, *Nature*  
771 *Geoscience* 1(10), 659-664.
- 772 Horiuchi, K., Uchida, T., Sakamoto, Y., Ohta, A., Matsuzaki, H., Shibata, Y., Motoyama, H.,  
773 2008. Ice core record of  $^{10}\text{Be}$  over the past millennium from Dome Fuji, Antarctica: a  
774 new record of past solar activity and a powerful tool for stratigraphic dating.  
775 *Quaternary Geochronology* 3, 253–261.
- 776 Jennings, A.E., Walton, M.E., Ó Cofaigh, C., Kilfeather, A.A., Andrews, J.T., Ortiz, J.D., de  
777 Vernal, A., Dowdeswell, J.A., 2013. Paleoenvironments during Younger Dryas-Early  
778 Holocene retreat of the Greenland Ice Sheet from outer Disko Trough, central west  
779 Greenland. *Journal of Quaternary Science* 29 (1): 27-40, doi:10.1002/jqs.2652.
- 780 Klassen, R.A., Fisher, D.A., 1988. Basal-flow conditions at the northeastern margin of the  
781 Laurentide Ice Sheet, Lancaster Sound. *Canadian Journal of Earth Sciences* 25 (11):  
782 1740–1750.
- 783 Knudsen, M.F., Henderson, G.M., Frank, M., Mac Niocaill, C., Kubik, P.W., 2008. In-phase  
784 anomalies in beryllium-10 production and palaeomagnetic field behaviour during the  
785 Iceland Basin geomagnetic excursion. *Earth and Planetary Science Letters* 265 (3-4):  
786 588-599, doi:10.1016/j.epsl.2007.10.051.
- 787 Korschinek, G., Bergmaier, A., Faestermann, T., Gerstmann, U.C., Knie, K., Rugel, G.,  
788 Wallner, A., Dillmann, I., Dollinger, G., Lierse von Gostomski, Ch., Kossert, K.,  
789 Maiti, M., Poutivtsev, M., Remmert, A., 2010. A new value for the half-life of  $^{10}\text{Be}$  by  
790 Heavy-Ion Elastic Recoil Detection and liquid scintillation counting. *Nuclear*  
791 *Instruments and Methods in Physics Research B.* 268 (2): 187-191.  
792 doi:10.1016/j.nimb.2009.09.020.
- 793 Kovaltsov, G.A., Usoskin, I.G., 2010. A new 3D numerical model of cosmogenic nuclide  
794  $^{10}\text{Be}$  production in the atmosphere. *Earth and Planetary Science Letters* 291 (1-4):  
795 182-188, doi:10.1016/j.epsl.2010.01.011.
- 796 Kusakabe, M., Ku, T.L., Southon, J.R., Liu, S., Vogel, J.S., Nelson, D.E., Nakaya, S.,  
797 Cusimano, G.L., 1991. Be isotopes in rivers/estuaries and their oceanic budgets. *Earth*  
798 *and Planetary Science Letters* 102 (3): 265-276.
- 799 Lal, D., Peters, B., 1967. Cosmic ray produced radioactivity on the Earth, in *Handbuch der*  
800 *Physik* (Springer, New York), vol. XLVI/2: 551–612.
- 801 Lal, D., 1988. Theoretically expected variations in the terrestrial cosmic-ray production rates  
802 of isotopes. In: Cini Castagnoli, G. (Ed.), *Solar–Terrestrial Relationships and the*  
803 *Earth Environment in the last Millennia.* Soc. Italiana di Fisica, Bologna, pp. 216–233.
- 804 Laj, C., Kissel, C., Mazaud, A., Channell, J.E.T., Beer, J., 2000. North Atlantic  
805 palaeointensity stack since 75 Ka (NAPIS-75) and the duration of the Laschamp  
806 event. *Philosophical Transactions of the Royal Society of London* 358 (1768): 1009-  
807 1025.
- 808 Lao, Y., Anderson, R.F., Broecker, W.S., 1992. Boundary scavenging and deep-sea sediment  
809 dating: constraints from excess  $^{230}\text{Th}$  and  $^{231}\text{Pa}$ . *Paleoceanography* 7 (6): 783-798.

- 810 Laskar, J., Robutel, P., Joutel, F., Gastineau, M., Correia, A.C.M., Levrard, B., 2004. A long-  
811 term numerical solution for the insolation quantities of the Earth. *Astronomy and*  
812 *Astrophysics* 428 (1): 261–85, doi:10.1051/0004-6361:20041335.
- 813 Li, G., Piper, D.J.W., Campbell, D.C., 2011. The Quaternary Lancaster Sound trough-mouth  
814 fan, NW Baffin Bay. *Journal of Quaternary Science* 26 (5): 511-522,  
815 doi:10.1002/jqs.1479.
- 816 Lisiecki, L.E., Lisiecki, P.A., 2002. Application of dynamic programming to the correlation  
817 of paleoclimate records. *Paleoceanography* 17 (4): 1049, doi:10.1029/2001PA000733.
- 818 Long, A.J., Roberts, D.H., Simpson, M.J.R., Dawson, S., Milne, G.A., Huybrechts, P., 2008.  
819 Late Weichselian relative sea-level changes and ice sheet history in southeast  
820 Greenland. *Earth and Planetary Science Letters* 272 (1-2): 8–18,  
821 doi:10.1016/j.epsl.2008.03.042.Long, 2008.
- 822 MacLean, B., 1985. Geology of the Baffin Island Shelf, in *Quaternary Environments: Eastern*  
823 *Canadian Arctic, Baffin Bay and Western Greenland*, edited by J.T. Andrews, pp.  
824 154–177, Allen and Unwin, Boston.
- 825 Marcott, S.A., Clark, P.U., Padman, L., Klinkhammer, G.P., Springer, S.R., Liu, Z., Otto-  
826 Bliesner, B.L., Carlson, A.E., Ungerer, A., Padman, J., 2011. Ice-shelf collapse from  
827 subsurface warming as a trigger for Heinrich events. *Proceedings of the National*  
828 *Academy of Sciences* 108 (33): 13415–13419, doi:10.1073/pnas.1104772108.
- 829 Margold, M., Stokes, C.R., Clark, C.D., 2015. Ice streams in the Laurentide Ice Sheet:  
830 Identification, characteristics and comparison to modern ice sheets. *Earth Science*  
831 *Reviews* 143: 117-146, doi:10.1016/j.earscirev.2015.01.011
- 832 Masarik, J., Beer, J. 1999. Simulation of particle fluxes and cosmogenic nuclide production in  
833 the Earth's atmosphere. *Journal of Geophysical Research* 104 (D10): 12099-12111.
- 834 Masarik, J., Beer, J. 2009. An updated simulation of particle fluxes and cosmogenic nuclide  
835 production in the Earth's atmosphere. *Journal of Geophysical Research* 114: D11103,  
836 doi:10.1029/2008JD010557.
- 837 Ménabréaz, L., Thouveny, N., Bourlès, D.L., Deschamps, P., Hamelin, B., Demory, F., 2011.  
838 The Laschamp geomagnetic dipole low expressed as a cosmogenic  $^{10}\text{Be}$  atmospheric  
839 overproduction at ~41ka. *Earth and Planetary Science Letters* 312 (3-4): 305-317,  
840 doi:10.1016/j.epsl.2011.10.037.
- 841 Ménabréaz, L., Bourlès, D.L., Thouveny, N., 2012. Amplitude and timing of the Laschamp  
842 geomagnetic dipole low from the global atmospheric  $^{10}\text{Be}$  overproduction:  
843 contribution of authigenic  $^{10}\text{Be}/^9\text{Be}$  ratios in west equatorial Pacific sediments. *Journal*  
844 *of Geophysical Research* 117: B11101, doi:10.1029/2012JB009256.
- 845 Ménabréaz, L., 2012, Production atmosphérique du nucléide cosmogénique  $^{10}\text{Be}$  et variations  
846 de l'intensité du champ magnétique terrestre au cours des derniers 800 000 ans. PhD  
847 Thesis, Aix-Marseille Université, pp. 292.
- 848 Ménabréaz, L., Thouveny, N., Bourlès, D.L., Vidal, L., 2014. The geomagnetic dipole  
849 moment variation between 250 and 800 ka BP reconstructed from the authigenic  
850  $^{10}\text{Be}/^9\text{Be}$  signature in West Equatorial Pacific sediments. *Earth and Planetary Science*  
851 *Letters*. *Earth and Planetary Science Letters* 385: 190-205,  
852 doi:10.1016/j.epsl.2013.10.037.
- 853 Monaghan, M.C., Krishnaswami, S., Turekian, K.K., 1986. The global-average production  
854 rate of  $^{10}\text{Be}$ . *Earth and Planetary Science Letters* 76: 279–287.

- 855 Murayama, M., Nagai, H., Imamura, M., Hatori, S., Kobayashi, K., Taira, A., 1997.  $^{10}\text{Be}$  and  
856  $^9\text{Be}$  concentrations in the deep sea sediment at site 925, Ceara Rise, in the western  
857 equatorial Atlantic: implication of  $^{10}\text{Be}$  flux change. Shackleton, N.J., Curry, W.B.,  
858 Richter, C., and Bralower, T.J. (Eds.). Proceedings of the Ocean Drilling Program,  
859 Scientific Results, Vol. 154: 389-394.
- 860 Muscheler, R., Beer, J., Wagner, G., Laj, C., Kissel, C., Raisbeck, G.M., Yiou, F., Kubik,  
861 P.W., 2004. Changes in the carbon cycle during the last deglaciation as indicated by  
862 the Comparison of  $^{10}\text{Be}$  and  $^{14}\text{C}$  records. Earth and Planetary Science Letters 219:  
863 325-340, doi:10.1016/S0012-821X(03)00722-2.
- 864 Muscheler, R., Beer, J., Kubik, P.W., Synal, H.A., 2005. Geomagnetic field intensity during  
865 the last 60,000 years based on  $^{10}\text{Be}$  and  $^{36}\text{Cl}$  from the Summit ice cores and  $^{14}\text{C}$ .  
866 Quaternary Science Reviews 24 (16-17): 1849-1860,  
867 doi:10.1016/j.quascirev.2005.01.012.
- 868 Nishiizumi, K., Imamura, M., Caffee, M.W., Southon, J.R., Finkel, R.C., McAninch, J., 2007.  
869 Absolute calibration of  $^{10}\text{Be}$  AMS standards. Nuclear Instruments and Methods in  
870 Physics Research Section B 258: 403–413.
- 871 Nuttin, L., Hillaire-Marcel, C., 2015. U- and Th-series isotopes in deep Baffin Bay sediments:  
872 Tracers of detrital sources and of contrasted glacial/interglacial sedimentary processes.  
873 Marine Geology 361: 1-10. doi:10.1016/j.margeo.2015.01.003.
- 874 Ó Cofaigh, C., Andrews, J.T., Jennings, A.E., Dowdeswell, J.A., Hogan, K.A., Kilfeather,  
875 A.A., Sheldon, C., 2012. Glacimarine lithofacies, provenance and depositional  
876 processes on a West Greenland trough-mouth fan. Journal of Quaternary Science 28  
877 (1): 13-26, doi:10.1002/jqs.2569.
- 878 Ó Cofaigh, C., Dowdeswell, J.A., Jennings, A.E., Hogan, K.A., Kilfeather, A.A., Hiemstra,  
879 J.F., Noormets, R., Evans, J., McCarthy, D.J., Andrews, J.T., Lloyd, J.M., Moros, M.,  
880 2013. An extensive and dynamic ice sheet on the West Greenland shelf during the last  
881 glacial cycle. Geology 41 (2): 219-222, doi:10.1130/G33759.1.
- 882 O'Brien, K., 1979. Secular variations in the production of cosmogenic isotopes in the Earth's  
883 atmosphere. Journal of Geophysical Research 84: 423–431.
- 884 O'Brien, K., de La Zerda Lerner, A., Shea, M., Smart, D., 1991. The production of  
885 cosmogenic isotopes in the Earth's atmosphere and their inventories. In: Sonett, C.P.,  
886 Giampapa, M.S., Matthews, M.S. (Eds.), The Sun in Time. The University of Arizona,  
887 pp. 317–342.
- 888 Pedro, J., Van Ommen, T.D., Curran, M.A.J., Morgan, V., Smith, A., Mc Morrow, A., 2006.  
889 Evidence for climate modulation of the  $^{10}\text{Be}$  solar activity proxy. Journal of  
890 Geophysical Research 111: D21105, doi:10.1029/2005JD006764.
- 891 Raisbeck, G.M., Yiou, F., Fruneau, M., Loiseaux, J.M., Lieuvain, M., Ravel, J.C., 1981.  
892 Cosmogenic  $^{10}\text{Be}/^7\text{Be}$  as a probe of atmospheric transport processes. Geophysical  
893 Research Letters 8 (9): 1015–1018, doi:10.1029/GL008i009p01015.
- 894 Raisbeck, G.M., Yiou, F., Bourlès, D., Kent, D.V., 1985. Evidence for an increase in  
895 cosmogenic  $^{10}\text{Be}$  during a geomagnetic reversal. Nature 315, 315–317,  
896 doi:10.1038/315315a0.
- 897 Raisbeck, G.M., Yiou, F., Jouzel, J., Petit, J.R., Bard, E., Barkov, N.I., 1992.  $^{10}\text{Be}$  deposition  
898 at Vostok, Antarctica, during the last 50000 years and its relationship to possible  
899 cosmogenic production variations during this period. In: Bard, E., Broecker, W.S.



- 900 (Eds.), *The Last Deglaciation: Absolute and Radiocarbon Chronologies, Series I.*  
 901 *Glob. Environmental Change* 2, pp. 127–139.
- 902 Raisbeck, G.M., Yiou, F., Cattani, O., Jouzel, J., 2006.  $^{10}\text{Be}$  evidence for the Matuyama–  
 903 Brunhes geomagnetic reversal in the EPICA Dome C ice core. *Nature* 444 (7115): 82–  
 904 84, doi:10.1038/nature05266.
- 905 Robinson, C., Raisbeck, G.M., Yiou, F., Lehman, B., Laj, C., 1995. The relationship between  
 906  $^{10}\text{Be}$  and geomagnetic field strength records in central North Atlantic sediments during  
 907 the last 80 ka. *Earth and Planetary Science Letters* 136 (3): 551–557,  
 908 doi:10.1016/0012-821X(95)00202-N.
- 909 Roy-Barman, M., Jeandel, C., Souhaut, M., Rutgers van der Loeff, M., Voege, I., Leblond,  
 910 N., Freydier, R., 2005. The influence of particle composition on thorium scavenging  
 911 in the NE Atlantic ocean (POMME Experiment). *Earth and Planetary Science Letters*  
 912 240 (3): 681–693.
- 913 Roy-Barman, M., 2009. Modelling the effect of boundary scavenging on Thorium and  
 914 Protactinium profiles in the ocean. *Biogeosciences* 6 (12): 3091–3107.
- 915 Sellén, E., Jakobsson, M., Frank, M., Kubik, P.W., 2009. Pleistocene variations of beryllium  
 916 isotopes in central Arctic Ocean sediment cores. *Global and Planetary Change* 68: 38–  
 917 47.
- 918 Simon, Q., St-Onge, G., Hillaire-Marcel, C., 2012. Late Quaternary chronostratigraphic  
 919 framework of deep Baffin Bay glaciomarine sediments from high-resolution paleo-  
 920 magnetic data. *Geochemistry, Geophysics, Geosystems* 13 (1-24): Q0A003,  
 921 doi:10.1029/2012GC004272.
- 922 Simon, Q., Hillaire-Marcel, C., St-Onge, G., Andrews, J.T., 2014. North-eastern Laurentide,  
 923 western Greenland and southern Inuitian ice stream dynamics during the last glacial  
 924 cycle. *Journal of Quaternary Science* 29 (1): 14–26, doi:10.1002/jqs.2648.
- 925 Simon Q. 2013. Propriétés magnétiques, minéralogiques et sédimentologique des sédiments  
 926 profond de la baie de Baffin: chronologie et dynamique des glaciers ouest  
 927 groenlandais, innuitiens et laurentidiens au cours de la dernière glaciation. PhD  
 928 Thesis, Université du Québec à Montreal, pp. 181.
- 929 Simon Q, Hillaire-Marcel C, St-Onge G. (in prep). Detrital carbonate events in Baffin Bay  
 930 during the last climatic cycle: Their timing vs. the Greenland Dansgaard-Oeschger  
 931 cycles and North Atlantic Heinrich events.
- 932 Simpson, M.J.R., Milne, G.A., Huybrechts, P., Long, A.J., 2009. Calibrating a glaciological  
 933 model of the Greenland Ice Sheet from the Last Glacial Maximum to present-day  
 934 using field observations of relative sea level and ice extent. *Quaternary Science*  
 935 *Reviews* 28 (17-18): 1631–57.
- 936 Sjunneskog, C., Scherer, R., Aldahan, A., Possnert, G., 2007.  $^{10}\text{Be}$  in glacial marine sediment  
 937 of the Ross Sea, Antarctica, a potential tracer of depositional environment and  
 938 sediment chronology. *Nuclear Instruments and Methods in Physics Research Section*  
 939 *B* 259 (1): 576–583, doi:10.1016/j.nimb.2007.01.203.
- 940 Spielhagen, R.F., Bonani, G., Eisenhauer, A., Frank, M., Frederichs, T., Kassens, H., Kubik,  
 941 P.W., Mangini, A., Nøgaard Pedersen, N., Nowaczyk, N.R., Schäper, S., Stein, R.,  
 942 Thiede, J., Tiedemann, R., Washner, M., 1997. Arctic Ocean evidence for late  
 943 Quaternary initiation of northern Eurasian ice sheets. *Geology* 25 (9): 783–786.

- 944 Steffensen, J.P., Andersen, K.K., Bigler, M., Clausen, H.B., Dahl-Jensen, D., Fischer, H.,  
945 Goto-Azuma, K., Hansson, M., Johnsen, S.J., Jouzel, J., Masson-Delmotte, V., Popp,  
946 T., Rasmussen, S.O., Röthlisberger, R., Ruth, U., Stauffer, B., Siggaard-Andersen,  
947 M.L., Sveinbjörnsdóttir, A.E., Svensson, A., White, J.W.C., 2008. High-Resolution  
948 Greenland Ice Core Data Show Abrupt Climate Change Happens in Few Years.  
949 *Science* 321 (5889): 680-684, doi:10.1126/science.1157707.
- 950 Steig, E.J., Polissar, P.J., Stuiver, M., Grootes, P.M., Finkel, R.C., 1996. Large amplitude  
951 solar modulation cycles of  $^{10}\text{Be}$  in Antarctica: Implications for atmospheric mixing  
952 processes and interpretation of the ice core record. *Geophysical Research Letters* 23  
953 (5): 523–526.
- 954 Stoner, J.S., Channell, J.E.T., Hillaire-Marcel, C., Kissel, C., 2000. Geomagnetic  
955 paleointensity and environmental record from Labrador Sea core MD95-2024: global  
956 marine sediment and ice core chronostratigraphy for the last 110 kyr. *Earth and  
957 Planetary Science Letters* 183 (1-2): 161-177.
- 958 Thouveny, N., 1988. High-resolution palaeomagnetic study of late Pleistocene sediments  
959 from Baffin Bay: first results. *Canadian Journal of Earth Sciences* 25: 833-843.
- 960 Thouveny, N., Bourlès, D.L., Saracco, G., Carcaillet, J.T., Bassinot, F., 2008. Paleoclimatic  
961 context of geomagnetic dipole lows and excursions in the Brunhes, clue for an orbital  
962 influence on the geodynamo?. *Earth and Planetary Science Letters* 275 (3-4): 269-284,  
963 doi:10.1016/j.epsl.2008.08.020.
- 964 Valet, J.P., Bassinot, F., Bouilloux, A., Bourlès, D.L., Nomade, S., Guillou, V., Lopes, F.,  
965 Thouveny, N., Dewilde, F., 2014. Geomagnetic, cosmogenic and climatic changes  
966 across the last geomagnetic reversal from Equatorial Indian Ocean sediments. *Earth  
967 and Planetary Science Letters* 397: 67-79, doi:10.1016/j.epsl.2014.03.053.
- 968 von Blanckenburg, F., O'Nions, R.K., Belshaw, N.S., Gibb, A., Hein, J.R., 1996. Global  
969 distribution of beryllium isotopes in deep ocean water as derived from Fe-Mn crusts.  
970 *Earth and Planetary Science Letters* 141 (1): 213–226.
- 971 von Blanckenburg, F., O'Nions, R.K., 1999. Response of beryllium and radiogenic isotope  
972 ratios in Northern Atlantic Deep Water to the onset of northern hemisphere glaciation.  
973 *Earth and Planetary Science Letters* 167 (3): 175-182.
- 974 von Blanckenburg, F., Bouchez, J., 2014. River fluxes to the sea from the ocean's  $^{10}\text{Be}/^{9}\text{Be}$   
975 ratio. *Earth and Planetary Science Letters* 387: 34–43.
- 976 Vogt, S., Herzog, G.F., Reedy, R.C., 1990. Cosmogenic nuclides in extraterrestrial materials.  
977 *Reviews of Geophysics* 28 (3): 253-275.
- 978 Wagner, G., Masarik, J., Beer, J., Baumgartner, S., Imboden, D., Kubik, P.W., Synal, H.A.,  
979 Suter, M., 2000. Reconstruction of the geomagnetic field between 20 and 60 kyr BP  
980 from cosmogenic radionuclides in the GRIP ice core. *Nuclear Instruments and  
981 Methods in Physics Research B* 172: 597-604
- 982 Webber, W.R., Soutoul, A., Kish, J.C., Rockstroh, J.M., 2003. Updated formula for  
983 calculating partial cross sections for nuclear reactions of nuclei with  $Z \leq 28$  and  $E >$   
984  $150$  MeV nucleon $^{-1}$  in hydrogen targets. *The Astrophysical Journal Supplement  
985 Series* 144: 153-167.
- 986 Webber, W.R., Higbie, P.R., McCracken, K.G., 2007. Production of the cosmogenic isotopes  
987  $^3\text{H}$ ,  $^7\text{Be}$ ,  $^{10}\text{Be}$ , and  $^{36}\text{Cl}$  in the Earth's atmosphere by solar and galactic cosmic rays.  
988 *Journal of Geophysical Research* 112: A10106, doi:10.1029/2007JA012499.

989 Werner, M., Tegen, I., Harrison, S.P., Kohfeld, K.E., Prentice, I.C., Balkanski, Y., Rodhe, H.,  
990 Roelandt, C., 2002. Seasonal and interannual variability of the mineral dust cycle  
991 under present and glacial climate conditions. *Journal of Geophysical Research* 107  
992 (D24), 4744, doi:10.1029/2002JD002365.

993 Yiou, F., Raisbeck, G.M., Bourlès, D.L., Lorius, C., Barkov, N.I., 1985.  $^{10}\text{Be}$  in ice at Vostok  
994 Antarctica during the last climatic cycle. *Nature* 316 (6029): 616-617.

995 Yiou, F., Raisbeck, G.M., Baumgartner, S., 1997. Beryllium 10 in the Greenland Ice Core  
996 Project ice core at Summit, Greenland. *Journal of Geophysical Research* 102 (C12):  
997 26783-26794.  
998

999 **Table 1.** AMS measurements, authigenic  $^{10}\text{Be}$  and  $^9\text{Be}$  concentrations, authigenic  $^{10}\text{Be}/^9\text{Be}$   
1000 ratios and calculated  $^{10}\text{Be}$ -fluxes of core HU2008-029-016PC samples.

1001 **Table 2.** Correlation coefficients of Be isotopes (concentration, ratio and fluxes) and  
1002 sedimentological parameters.

1003 **Table 3.**  $^{10}\text{Be}$ -production/flux in literature (in  $\text{atoms}\cdot\text{cm}^{-2}\cdot\text{kyr}^{-1}$ )  
1004

1005 **Figure 1.** General bathymetry, simplified oceanic circulation, sketch of the Paleozoic  
1006 outcrops (*MacLean*, 1985) and paleo-Ice-Sheets (including LGM unknown maximum ice  
1007 margin extents) of the Baffin Bay region. The location of HU2008-029-016PC sampling site  
1008 is indicate by a red dots. Red arrows illustrate Atlantic “warm” waters, whereas the blue  
1009 arrows represent colder Arctic waters. The simplified representations of the Greenland  
1010 (green), Innuitian (blue) and Laurentide ice sheet (red) limits and major ice stream locations  
1011 during the LGM (colored areas) are adapted from *Funder et al.* (2011), *Dyke* (2004) and  
1012 *England et al.* (2006).

1013 **Figure 2.** Relative paleointensity (NRM/ARM<sub>25-35mT</sub>) tuned on RPI record of ODP Site 1063  
1014 (*Channell et al.*, 2012) and chronostratigraphy of PC16. The RPI tie-points used in this study  
1015 are represented by green dots while the red diamonds and yellow triangle are radiocarbon  
1016 ages and calcite tie-points respectively (*Simon et al.*, 2012). The incertitude in the age model  
1017 is represented by shaded area.

1018 **Figure 3.** Beryllium isotopes results vs. high-resolution physical, geochemical and  
1019 mineralogical results from core PC16. Log: general simplified stratigraphy of the core; CT:  
1020 CAT-Scan image of the core; HRI: high-resolution digital image; CT Number (density  
1021 proxy); XRD carbonates (dolomite and calcite) cumulative percents; log(Ca/Fe):  $\mu\text{XRF}$   
1022 element ratio for calcium and iron measured with the ITRAX© core scanner. Grain size (%)  
1023 for clay, silt fractions and coarse fractions measured at 4 cm intervals by laser diffraction.  
1024 Authigenic  $^{10}\text{Be}$ ,  $^9\text{Be}$  and  $^{10}\text{Be}/^9\text{Be}$  ratios are display in log scale. Distinct lithological facies

1025 are highlighted with color banding. Red: uppermost brownish gray silty mud unit (Uppermost  
1026 Brownish, “UB”); light green: olive-black silty to clayey mud unit (Olive Clay, “OC”); white:  
1027 carbonate-rich yellowish-brown to dark- brown very poorly sorted gravelly sandy mud  
1028 detrital layers (DC); dark green: olive gray to dark gray poorly sorted silty to sandy mud low  
1029 carbonate detrital layers (LDC) (see text for details).

1030 **Figure 4.** Principal component analysis (PCA) of the mineralogical and grain-size dataset.  
1031 The loading scores for PC1 vs. PC2 explain, respectively, 61 and 11.5% of the total variance.  
1032 PCA analysis illustrates the two sedimentary modes in Baffin Bay.

1033 **Figure 5.** Authigenic  $^{10}\text{Be}/^9\text{Be}$  ratios and  $^{10}\text{Be}$ -fluxes on depth. The  $^{10}\text{Be}$ -fluxes are compared  
1034 to references: (1) global-average  $^{10}\text{Be}$ -production values from models, see Table 3 for values  
1035 and references (the blue star is the mean value from Masarik and Beer, 2009); (2) global  
1036 values measured and averaged by Monaghan *et al.*, 1986; (3)  $^{10}\text{Be}$ -flux in GRIP/GISP2 ice  
1037 core (Muscheler *et al.*, 2005); (4)  $^{10}\text{Be}$ -flux in marine records representing the so-called  
1038 “allowed range” from Christl *et al.*, 2007, 2010; (5)  $^{10}\text{Be}$ -flux range in deep sea sedimentary  
1039 cores from the Arctic Ocean and the Norwegian Sea (Eisenhauer *et al.*, 1994). Red (resp.  
1040 blue) dots represent measured  $^{230}\text{Th}_{\text{xs}}$  vertical flux higher (resp. lower) than theoretical  $^{230}\text{Th}_{\text{xs}}$   
1041 vertical flux.

1042 **Figure 6.** Authigenic  $^{10}\text{Be}/^9\text{Be}$  ratios vs.  $^{10}\text{Be}$ -fluxes ( $^{230}\text{Th}_{\text{xs}}$ -normalized). Blue dots represent  
1043 measured  $^{230}\text{Th}_{\text{xs}}$ -flux samples lower than theoretical flux and illustrate episodes of Arctic  
1044 Waters outflow through Davis Strait (Nuttin and Hillaire-Marcel, 2015).

1045 **Figure 7.** Authigenic  $^{10}\text{Be}/^9\text{Be}$  ratios,  $^{10}\text{Be}$ -fluxes ( $^{230}\text{Th}_{\text{xs}}$ -normalized), PC 1 and RPI vs. age.  
1046 RPI (Channell *et al.*, 2012) and  $^{10}\text{Be}$ -fluxes (Christl *et al.*, 2010) from ODP Site 1063 are  
1047 presented along with  $^{10}\text{Be}$ -fluxes reference ranges from distinct archives and models (see  
1048 Figure 5 and Table 3 for references). Marine isotopic stages 1 to 6 are represented by color  
1049 boxes along the age axis. BBDC-layers are represented by a vertical grey banding and  
1050 numbered according to Simon *et al.* (in prep.).

1051 **Figure 8.** Paleoclimatic interpretations of authigenic  $^{10}\text{Be}/^9\text{Be}$  ratio variations. The NGRIP  
1052  $\delta^{18}\text{O}$  ice core record (red curves) and synthetic Greenland record (GLT-syn, blue curve) are  
1053 from [www.icecores.dk](http://www.icecores.dk) and Barker *et al.* (2011). Marine isotope stages 1 to 6 are represented  
1054 with color boxes. BBDC-layers (defined by high XRD carbonates cumulative percents) are  
1055 represented by the grey vertical bars and numbered according to Simon *et al.*, (in prep.). The  
1056 North Atlantic Heinrich events (Hemming, 2004) are indicated for comparison. The July  
1057 insolation is calculated at  $70^\circ\text{N}$  (from Laskar *et al.*, 2004). Eustatic relative sea level (RSL) is  
1058 from Grant *et al.* (2012). SIRM/ $k_{\text{LF}}$  is a magnetic grain size proxy (Simon *et al.*, 2012, in

1059 prep.). The cumulative inventory ratio compares the  $^{230}\text{Th}_{\text{xs}}$  accumulation fluxes with the  
1060 theoretical vertical production in the overlying water column. Values below 1 during the  
1061 Holocene indicate  $^{230}\text{Th}_{\text{xs}}$ -losses while values above 1 during the glacial period suggest a  
1062 sediment-focusing environment (Nuttin and Hillaire-Marcel, 2015).

1063 **Figure 9.** Simplified Baffin Bay paleogeography during the last glacial cycle. (a) Trans-  
1064 Baffin drift characterized by IRD sediments originating from the northern ice streams, and by  
1065 meltwater sediment-laden plumes from Baffin Island ice streams. (b) Extended ice margins  
1066 characterized by Greenland and Baffin Island glacial flour sediments corresponding to a  
1067 permanently ice-covered bay, and by extended ice margin limits over continental shelves.

**Table 1.** AMS measurements, authigenic  $^{10}\text{Be}$  and  $^9\text{Be}$  concentrations, authigenic  $^{10}\text{Be}/^9\text{Be}$  ratios and calculated  $^{10}\text{Be}$ -fluxes of core HU2008-029-016PC samples.

Depth in core (cm)	Age Model 17/07/14B (ka cal BP)	Sample weight (g)	Measured $^{10}\text{Be}/^9\text{Be}$ ( $10^{-11}$ )*	Authigenic decay corrected [ $^{10}\text{Be}$ ] ( $10^6$ at/g)*	Authigenic [ $^9\text{Be}$ ] ( $10^{16}$ at/g)*	Authigenic $^{10}\text{Be}/^9\text{Be}$ ( $10^{-8}$ )*	Flux $^{10}\text{Be}$ Th_norm. <sup>a</sup> ( $10^8$ atoms.cm $^{-2}$ kyr $^{-1}$ )
0.5	0.80	0.994	3.011 ± 0.040	6.403 ± 0.085	3.269 ± 0.065	1.959 ± 0.094	7.753 ± 0.131
8.5	4.85	0.963	1.976 ± 0.029	4.326 ± 0.064	3.060 ± 0.054	1.417 ± 0.065	8.571 ± 0.181
16.5	9.68	1.000	0.797 ± 0.013	1.687 ± 0.027	1.930 ± 0.029	0.878 ± 0.038	6.522 ± 0.157
24.5	10.83	1.000	0.144 ± 0.003	0.304 ± 0.007	1.229 ± 0.011	0.249 ± 0.012	2.021 ± 0.063
32.5	10.98	0.990	0.218 ± 0.006	0.468 ± 0.012	1.048 ± 0.007	0.449 ± 0.024	3.044 ± 0.107
40.5	11.41	0.983	0.060 ± 0.002	0.129 ± 0.004	0.898 ± 0.029	0.144 ± 0.013	0.837 ± 0.028
48.5	11.91	0.988	0.038 ± 0.001	0.081 ± 0.003	0.740 ± 0.013	0.110 ± 0.008	1.916 ± 0.174
56.5	12.13	0.961	0.089 ± 0.002	0.195 ± 0.005	1.028 ± 0.023	0.191 ± 0.013	3.756 ± 0.363
64.5	12.76	1.074	0.408 ± 0.008	0.801 ± 0.016	1.090 ± 0.009	0.740 ± 0.032	
72.5	13.39	0.932	0.526 ± 0.009	1.191 ± 0.021	1.508 ± 0.029	0.795 ± 0.041	
80.5	13.93	1.014	0.159 ± 0.005	0.330 ± 0.010	0.973 ± 0.026	0.342 ± 0.028	4.242 ± 0.300
88.5	14.31	0.992	0.101 ± 0.003	0.215 ± 0.006	0.966 ± 0.007	0.224 ± 0.013	1.313 ± 0.052
96.5	14.68	0.971	0.061 ± 0.002	0.133 ± 0.004	0.810 ± 0.023	0.166 ± 0.014	1.084 ± 0.046
112	15.43	1.086	2.647 ± 0.036	5.151 ± 0.070	2.507 ± 0.054	2.070 ± 0.105	15.755 ± 0.432
128.5	17.61	0.970	1.033 ± 0.015	2.233 ± 0.033	1.554 ± 0.016	1.450 ± 0.052	11.781 ± 0.392
136.5	18.30	1.003	2.048 ± 0.030	4.321 ± 0.064	2.150 ± 0.039	2.028 ± 0.095	12.817 ± 0.237
152.5	19.36	1.023	1.251 ± 0.021	2.582 ± 0.044	1.940 ± 0.039	1.344 ± 0.070	9.189 ± 0.197
168.5	20.43	1.012	0.682 ± 0.012	1.434 ± 0.026	0.949 ± 0.012	1.527 ± 0.066	10.225 ± 0.316
184.5	23.04	0.985	1.280 ± 0.020	2.762 ± 0.043	2.385 ± 0.072	1.172 ± 0.080	24.724 ± 0.829
200.5	25.41	0.987	1.934 ± 0.028	4.099 ± 0.060	1.777 ± 0.043	2.336 ± 0.132	17.374 ± 0.354
208.5	26.15	0.965	1.219 ± 0.017	2.660 ± 0.038	1.855 ± 0.045	1.453 ± 0.081	12.758 ± 0.281
218.5	27.05	0.978	0.252 ± 0.007	0.539 ± 0.015	0.709 ± 0.006	0.771 ± 0.045	
232.5	28.54	1.015	0.025 ± 0.001	0.051 ± 0.002	0.692 ± 0.007	0.074 ± 0.006	0.717 ± 0.046
248.5	34.55	0.964	0.032 ± 0.001	0.070 ± 0.002	0.590 ± 0.005	0.120 ± 0.008	0.989 ± 0.067
256.5	35.79	1.012	0.075 ± 0.002	0.153 ± 0.005	1.323 ± 0.036	0.118 ± 0.010	0.899 ± 0.034
264.5	37.57	0.950	0.048 ± 0.001	0.105 ± 0.003	1.178 ± 0.021	0.091 ± 0.006	1.762 ± 0.165
271	39.56	0.956	0.028 ± 0.001	0.062 ± 0.002	1.372 ± 0.017	0.046 ± 0.003	
273	40.13	0.955	0.023 ± 0.001	0.051 ± 0.002	1.233 ± 0.017	0.043 ± 0.003	2.401 ± 0.602
275	40.70	0.986	0.037 ± 0.001	0.079 ± 0.003	1.372 ± 0.034	0.058 ± 0.005	
277	41.33	0.955	0.333 ± 0.007	0.729 ± 0.016	1.426 ± 0.009	0.522 ± 0.023	
279	41.89	0.983	0.862 ± 0.014	1.846 ± 0.031	1.366 ± 0.024	1.380 ± 0.066	
281	42.34	0.967	0.968 ± 0.017	2.084 ± 0.037	1.293 ± 0.025	1.646 ± 0.086	
283	42.79	0.986	1.560 ± 0.024	3.333 ± 0.051	1.531 ± 0.035	2.224 ± 0.121	
285	43.35	0.996	1.941 ± 0.027	4.085 ± 0.058	1.860 ± 0.010	2.244 ± 0.067	
287	44.02	0.970	2.126 ± 0.031	4.584 ± 0.069	1.880 ± 0.015	2.492 ± 0.083	
289	44.69	0.998	2.227 ± 0.031	4.658 ± 0.067	2.081 ± 0.020	2.288 ± 0.078	
291	45.37	0.990	1.951 ± 0.030	4.135 ± 0.064	1.878 ± 0.010	2.252 ± 0.072	
293	46.04	0.999	1.689 ± 0.024	3.542 ± 0.051	1.790 ± 0.021	2.025 ± 0.074	
295	46.71	0.981	1.465 ± 0.021	3.134 ± 0.046	1.682 ± 0.007	1.907 ± 0.057	7.649 ± 0.165
304.5	49.00	0.977	0.993 ± 0.015	2.133 ± 0.033	0.990 ± 0.015	2.208 ± 0.095	21.963 ± 1.496
320.5	51.65	0.985	0.190 ± 0.006	0.405 ± 0.014	0.936 ± 0.008	0.444 ± 0.030	1.612 ± 0.046
336.5	53.84	0.974	2.280 ± 0.032	4.900 ± 0.070	2.003 ± 0.052	2.512 ± 0.149	25.388 ± 0.973
344.5	54.87	0.975	1.675 ± 0.024	3.610 ± 0.052	1.834 ± 0.032	2.023 ± 0.101	19.291 ± 0.837
352.5	55.89	0.980	2.183 ± 0.030	4.684 ± 0.067	1.977 ± 0.051	2.437 ± 0.143	18.556 ± 0.648
360.5	57.14	0.986	1.607 ± 0.023	3.438 ± 0.052	1.693 ± 0.013	2.089 ± 0.068	8.181 ± 0.145
368.5	59.01	0.998	0.141 ± 0.002	0.293 ± 0.005	0.812 ± 0.013	0.372 ± 0.017	2.325 ± 0.092
384.5	61.05	0.975	0.116 ± 0.003	0.247 ± 0.008	0.851 ± 0.010	0.299 ± 0.019	1.545 ± 0.066
392.5	62.07	0.976	0.148 ± 0.004	0.320 ± 0.010	0.920 ± 0.009	0.359 ± 0.022	2.133 ± 0.084
400.5	63.09	0.969	0.086 ± 0.003	0.186 ± 0.006	0.861 ± 0.024	0.223 ± 0.019	1.712 ± 0.098
408.5	64.88	1.002	0.110 ± 0.003	0.229 ± 0.007	0.925 ± 0.004	0.256 ± 0.016	1.916 ± 0.097
416.5	67.06	0.992	0.119 ± 0.003	0.250 ± 0.007	0.811 ± 0.005	0.319 ± 0.018	6.284 ± 0.929
418	67.61	0.986	0.071 ± 0.002	0.151 ± 0.005	0.621 ± 0.004	0.251 ± 0.015	
420	68.16	0.973	0.098 ± 0.003	0.210 ± 0.006	0.832 ± 0.016	0.261 ± 0.018	
422	68.70	0.978	0.103 ± 0.003	0.220 ± 0.006	0.847 ± 0.018	0.268 ± 0.018	1.934 ± 0.096
437	74.35	0.956	1.438 ± 0.022	3.164 ± 0.051	1.517 ± 0.027	2.164 ± 0.103	
440.5	75.62	0.979	1.888 ± 0.027	4.025 ± 0.061	1.809 ± 0.050	2.310 ± 0.144	4.189 ± 0.065
456.5	78.58	1.002	2.212 ± 0.032	4.653 ± 0.070	1.844 ± 0.034	2.624 ± 0.123	12.908 ± 0.292
472.5	81.21	0.974	0.283 ± 0.006	0.606 ± 0.014	1.331 ± 0.008	0.474 ± 0.022	3.461 ± 0.133
504.5	87.96	0.954	0.066 ± 0.001	0.144 ± 0.003	0.793 ± 0.009	0.189 ± 0.008	3.166 ± 0.548
520.5	92.17	0.973	0.788 ± 0.013	1.708 ± 0.031	1.521 ± 0.021	1.176 ± 0.052	17.334 ± 1.213
536.5	94.76	0.973	0.116 ± 0.003	0.248 ± 0.007	0.839 ± 0.011	0.310 ± 0.018	1.558 ± 0.073
552.5	97.35	1.000	0.058 ± 0.002	0.122 ± 0.004	0.798 ± 0.005	0.160 ± 0.010	0.743 ± 0.033
568.5	99.94	0.993	0.067 ± 0.002	0.140 ± 0.004	0.774 ± 0.007	0.191 ± 0.012	1.355 ± 0.096
584.5	102.62	0.990	0.075 ± 0.002	0.160 ± 0.005	0.841 ± 0.009	0.200 ± 0.013	0.867 ± 0.035
590	104.15	0.994	0.051 ± 0.002	0.107 ± 0.004	0.705 ± 0.007	0.160 ± 0.011	
600	107.33	0.974	1.051 ± 0.015	2.271 ± 0.035	1.302 ± 0.006	1.840 ± 0.057	17.365 ± 0.764
616.5	112.56	0.991	0.401 ± 0.007	0.849 ± 0.015	1.068 ± 0.025	0.841 ± 0.048	2.025 ± 0.053
632.5	116.84	0.990	0.496 ± 0.008	1.054 ± 0.019	1.123 ± 0.010	0.995 ± 0.038	4.881 ± 0.174
648.5	119.84	0.989	1.361 ± 0.020	2.899 ± 0.045	1.476 ± 0.025	2.085 ± 0.094	
664.5	122.96	0.990	0.127 ± 0.004	0.270 ± 0.009	0.771 ± 0.012	0.372 ± 0.025	1.204 ± 0.041
680.5	126.77	0.974	0.079 ± 0.002	0.171 ± 0.005	0.782 ± 0.003	0.233 ± 0.014	
704.5	131.75	0.976	0.290 ± 0.007	0.627 ± 0.015	1.338 ± 0.023	0.501 ± 0.029	
720.5	134.25	0.991	0.488 ± 0.010	1.036 ± 0.022	1.051 ± 0.014	1.054 ± 0.050	
736.5	136.17	0.992	0.460 ± 0.008	0.977 ± 0.019	0.956 ± 0.017	1.094 ± 0.057	
Mean ± std. dev.			0.771 ± 0.823	1.639 ± 1.739	1.331 ± 0.561	1.009 ± 0.859	6.941 ± 7.037
Mean ± SDOM				1.639 ± 0.202	1.331 ± 0.065	1.009 ± 0.100	6.941 ± 0.985
Replicate measurements <sup>b</sup>							
16.5	9.683	0.973	0.790 ± 0.015	1.708 ± 0.032	1.973 ± 0.023	0.870 ± 0.038	6.605 ± 0.161
184.5	23.041	0.987	1.315 ± 0.022	2.806 ± 0.047	2.578 ± 0.062	1.101 ± 0.064	25.112 ± 0.844
Blank			(x 10 $^{-11}$ )				
bk1			0.00071				
bk2			0.00120				
bk3			0.00089				
bk4			0.00148				
bk5			0.00067				
bk6			0.00053				

<sup>a</sup>normalisation using  $^{230}\text{Th}_{\text{ss}}$  (see Nuttin and Hillaire-Marcel, 2015 for  $^{230}\text{Th}_{\text{ss}}$  results)<sup>b</sup>new leachates

\*2-sigma uncertainties.

Table2

**Table 2.** Correlation coefficients of Be isotopes (concentration, ratio and fluxes) and sedimentological parameters.

Parameters	<sup>9</sup> Be (at./g)	<sup>10</sup> Be (at./g)	Rapport <sup>10</sup> Be/ <sup>9</sup> Be	<sup>230</sup> (Th <sub>xs</sub> ) <sup>0</sup> (dpm.g <sup>-1</sup> )	Flux- <sup>10</sup> Be Th_norm. (atoms.cm <sup>-2</sup> .kyr <sup>-1</sup> )	PC1	PC2
SAR 170714B (cm/kyr)	n.s.	n.s.	n.s.	n.s.	n.s.	n.s.	n.s.
XRD- Quartz (%)	0.51	0.50	0.49	n.s.	0.49	-0.68	n.s.
XRD- K-Feldspar (%)	0.55	0.69	0.75	n.s.	0.66	-0.77	n.s.
XRD- Plagioclase (%)	0.54	0.72	0.80	n.s.	0.71	-0.84	n.s.
XRD- Calcite (%)	-0.62	-0.72	-0.76	n.s.	-0.66	0.80	n.s.
XRD- Dolomite (%)	-0.51	-0.68	-0.74	n.s.	-0.71	0.89	n.s.
XRF- Ca/Fe	-0.73	-0.80	-0.81	0.55	-0.68	0.95	n.s.
XRF- K/Ti	-0.66	-0.74	-0.77	0.42	-0.65	0.85	n.s.
XRF- Ti/Ca	0.71	0.78	0.79	0.51	0.67	-0.94	n.s.
XRF- Ca	-0.71	-0.78	-0.77	0.54	-0.66	0.92	n.s.
XRF- Fe	0.69	0.77	0.81	0.53	0.66	-0.91	n.s.
GS- 0-2 μm (%)	n.s.	n.s.	0.40	n.s.	0.39	-0.58	0.74
GS- 2-4 μm (%)	0.73	0.77	0.72	0.51	0.61	-0.86	0.47
GS- 4-8 μm (%)	0.79	0.78	0.67	0.62	0.55	-0.82	0.48
GS- 8-63 μm (%)	n.s.	n.s.	n.s.	0.00	n.s.	n.s.	n.s.
GS- >63 μm (%)	-0.70	-0.73	-0.63	0.61	-0.51	0.76	-0.50
Density (g.cm <sup>-3</sup> )	-0.77	-0.76	-0.73	0.58	-0.66	0.77	n.s.
<sup>9</sup> Be (at)	<b>1.00</b>	0.88	0.71	0.72	0.60	-0.81	n.s.
<sup>10</sup> Be (at)	0.88	<b>1.00</b>	0.94	0.68	0.73	-0.89	n.s.
Ratio <sup>10</sup> Be/ <sup>9</sup> Be	0.71	0.94	<b>1.00</b>	0.50	0.81	-0.88	n.s.
<sup>230</sup> (Th <sub>xs</sub> ) <sup>0</sup> (dpm.g <sup>-1</sup> )	0.72	0.68	0.50	<b>1.00</b>	n.s.	-0.54	n.s.
Flux- <sup>10</sup> Be sed. (atoms.cm <sup>-2</sup> .kyr <sup>-1</sup> )	0.60	0.73	0.81	n.s.	<b>1.00</b>	-0.75	n.s.
PC1 Sedimentological parameter	-0.81	-0.89	-0.88	-0.54	-0.71		
PC2 Sedimentological parameter	n.s.	n.s.	n.s.	n.s.	n.s.		

n.s. are not significant (P &lt; 0.001)






**Table 3.**  $^{10}\text{Be}$ -production/flux in literature (in  $\text{atoms.cm}^{-2}.\text{kyr}^{-1}$ )




Range (x $10^8$ )	Mean values (x $10^8$ )	Notes	References
<b><math>^{10}\text{Be}</math>-production</b>			
5.7 - 10		Global average $^{10}\text{Be}$ -production (model)	<i>Webber et al., 2007; Masarik and Beer, 1999,</i>
12 - 19		60-90°N $^{10}\text{Be}$ -production (model)	<i>2009; Kovaltsov and Usoskin, 2010</i>
	6.6	Global average $^{10}\text{Be}$ -production (model)	<i>Masarik and Beer, 2009</i>
5.2 - 26.4	12.1	Global average $^{10}\text{Be}$ -production (analytical)	<i>Monaghan et al., 1986 (from precipitation</i>
11 - 17	14.0	Long term averaged glob. av. $^{10}\text{Be}$ -prod. (analytical)	<i>measurements during the year 1980)</i>
			<i>Webber and Higbie, 2003; Webber et al., 2007</i>
	6.0	Global average $^{10}\text{Be}$ -production (model)	
	14.2	Global average $^{10}\text{Be}$ -production (empiric)	<i>Lal and Peters, 1967</i>
	9.5	Global average $^{10}\text{Be}$ -production (analytical)	<i>O'Brien, 1979; O'Brien et al., 1991</i>
	12.6	Global average $^{10}\text{Be}$ -production (empiric)	<i>Lal, 1988</i>
<b><math>^{10}\text{Be}</math>-flux in ice-core records</b>			
1.8 - 8.6	3.4	Greenland Summit (GRIP/GISP2)	<i>Muscheler et al., 2005; Finkel and Nishiizumi, 199.</i>
	3.3	Dye 3 (Greenland)	<i>Beer et al., 1991</i>
1.5 - 12.8		Renland Ice Core over 1931-1987 (Greenland)	<i>Aldahan et al., 1998</i>
1.4 - 10		Dronning Maud Land ice core over 1932-1988 (Antarctic)	
	4.0±0.3	EPICA DML (Neumayer surface snow, Antarctic)	<i>Auer et al., 2009</i>
	1.9±0.1	EPICA DML (Kohnen deep ice core, Antarctic)	
	1.4±0.2	Dome C (surface firn and firn core 0-12 m; Antarctica)	
1.2 - 2.5		Epica DC between 320-340 kyr	<i>Cauquoin et al., 2014</i>
0.6 - 3.3	1.6	Epica DC between 200-800 kyr	<i>Cauquoin, 2013</i>
	2.5	Vostok, South Pole (Antarctic)	<i>Raisbeck and Yiou, 1985</i>
	1.4	Taylor Dome (Antarctic)	<i>Steig et al., 1996</i>
	1.7 and 1.8	Concordia and Vostok over the last 60 years (Antarctic)	<i>Baroni et al., 2011</i>
	4.8±1.6	Law Dome snow pit over the year 2001 (Antarctic)	<i>Pedro et al., 2006</i>
2.0 - 4.5		Dome Fuji ice core over 700-1900 yr CE (Antarctica)	<i>Horiuchi et al., 2008</i>
	2.2 (2.3)	GRIP snow pit (Greenland) $^{10}\text{Be}$ deposition flux (1986-1998)	<i>Heikkilä et al., 2008</i>
	2.8	ECHAM5-HAM general circulation model $^{10}\text{Be}$ deposition	
<b><math>^{10}\text{Be}</math>-flux in marine records</b>			
8.2 - 31.1	16.3	ODP1063 (Bermuda Rise): 0-250 kyr BP	<i>Christl et al., 2007, 2010</i>
7.8 - 37.1	16.1	ODP983 (North Atlantic): 0-250 kyr BP	
9 - 28		Globally intergrated / long-term averaged $^{10}\text{Be}$ -fluxes	
15 - 35		ODP 1063A (Bermuda Rise): 170-200 kyr BP, IB exc.	<i>Knudsen et al., 2008</i>
10 - 70		ODP 983B (North Atlantic): 170-200 kyr BP, IB exc.	
5 - 27		ODP 925 (Ceara Rise): 0-7 Ma	<i>Murayama et al., 1997</i>
5 - 60		Globally stacked deep-sea sediments: 0-200 kyr BP	<i>Frank et al., 1997</i>
6 - 7		ACEX average $^{10}\text{Be}$ -flux for the past 12.3 Ma (Actic)	<i>Frank et al., 2008</i>
31.9 - 65.9	40.9	Portuguese Margin (20-45 kyr BP)	<i>Ménabréaz et al., 2011</i>
2 - 23		Four Arctic Ocean cores (F=C x S x D)	<i>Eisenhauer et al., 1994; Aldahan et al., 1997</i>
<b><math>^{10}\text{Be}</math>-flux in PC16 (Baffin Bay marine sediments)</b>			
0.7 - 25.4 (1 - 35.5)	6.9 (9.7)	(values corrected)*	<i>This study</i>
<b>fluxes by facies:</b>			
6.5 - 8.6 (9.1 - 12)	7.6 (10.7)	Facies UB (Holocene)	
0.7 - 6.3 (1 - 8.8)	2 (2.8)	Facies BBDC (coarse carbonate-rich sediments)	
4.2 - 25.4 (5.8 - 35.5)	14.5 (20.2)	Facies LDC (fine feldspar-rich sediments)	
9.2 - 24.7 (12.8 - 34.6)	14.1 (19.8)	Facies OC (very fine feldspar-rich sediments)	

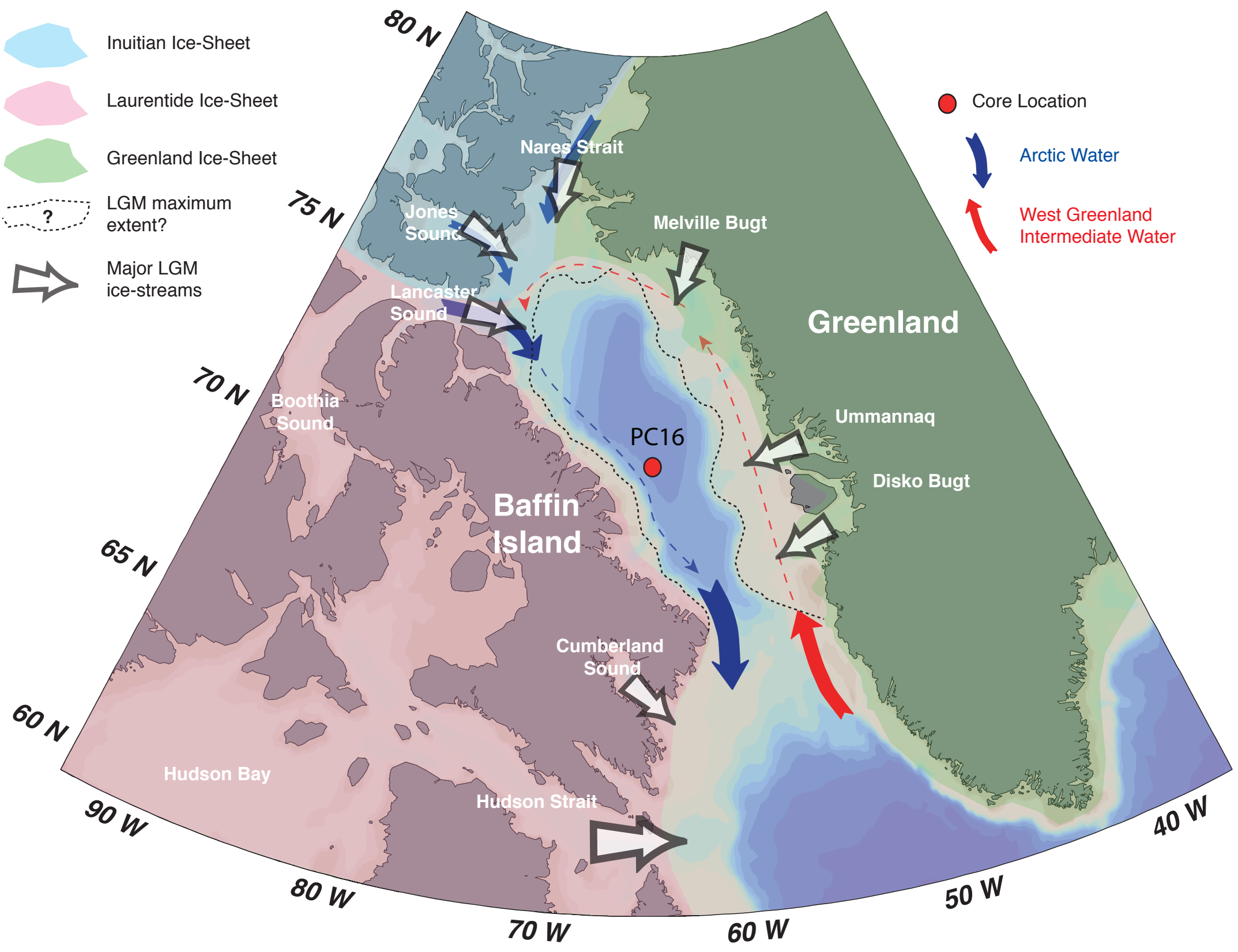
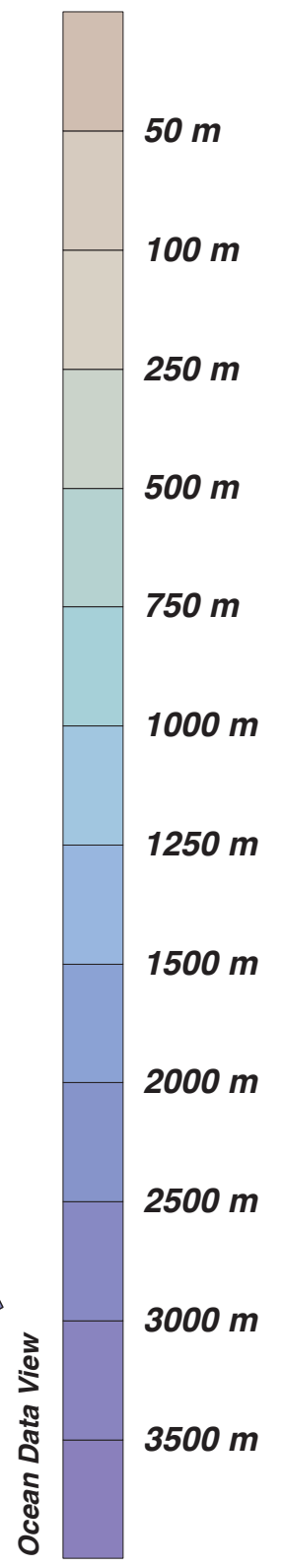
\*correction to encompass the underestimation of the flux due to methodological biases, see text for details

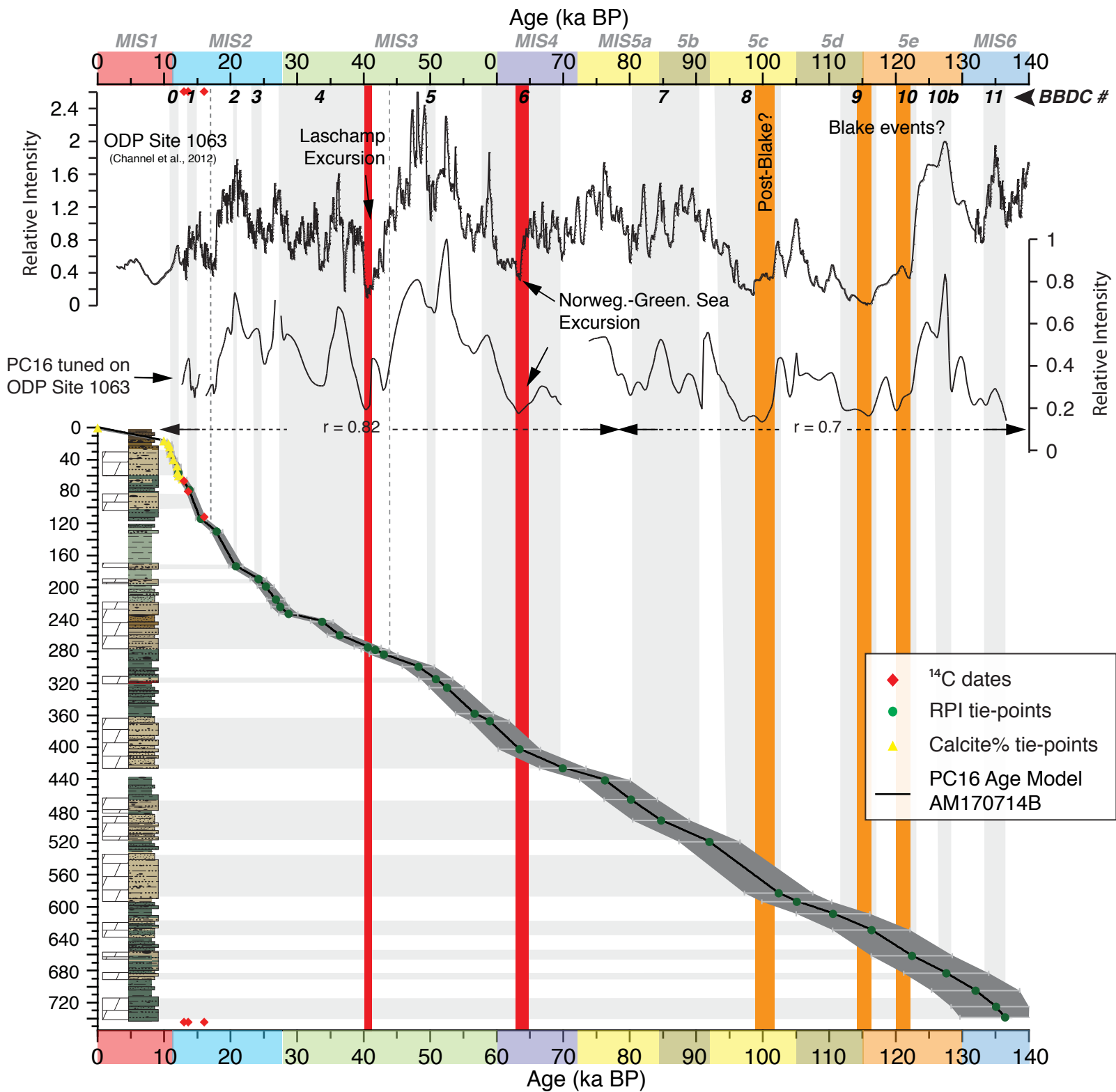


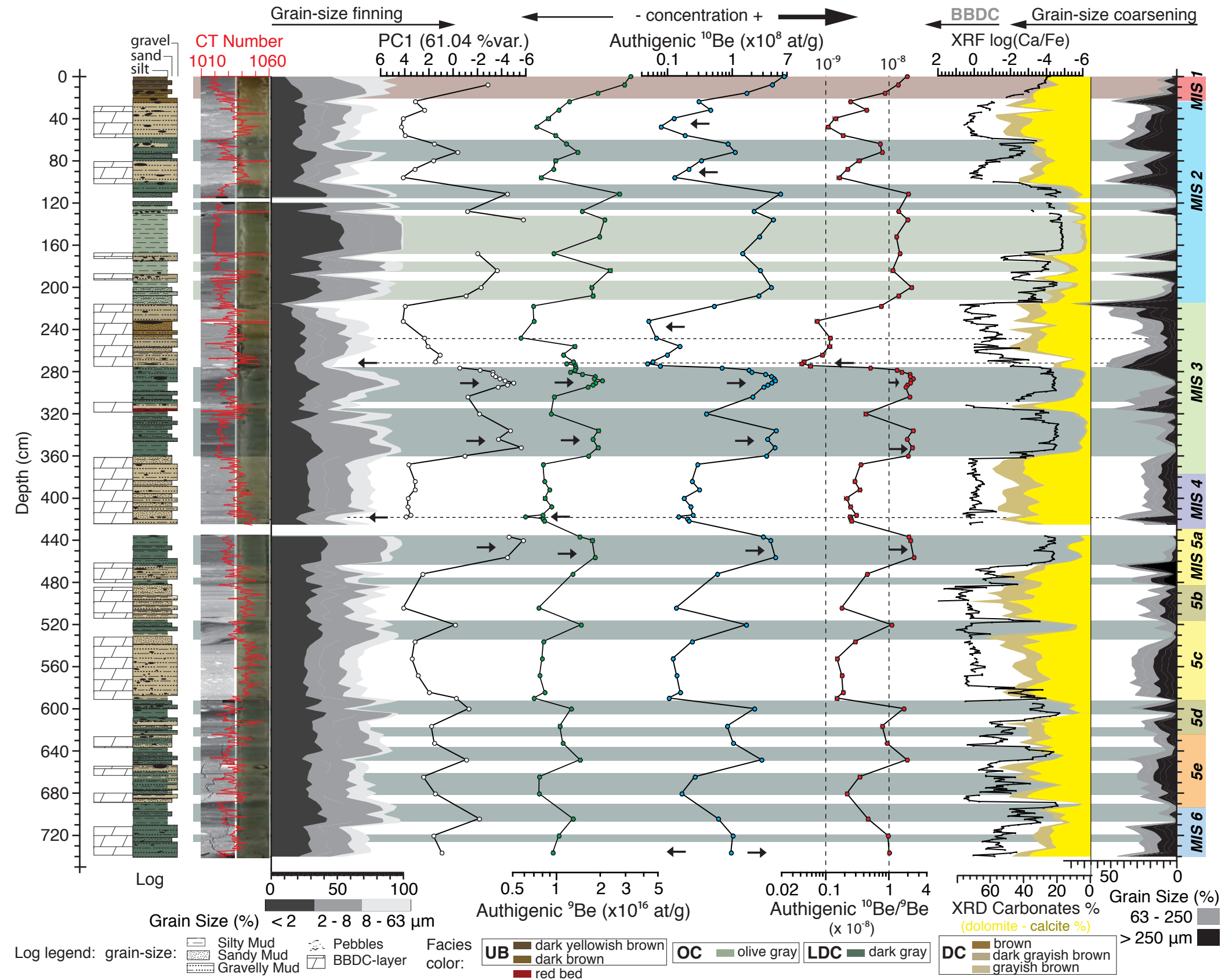
Figure

-  Inuitian Ice-Sheet
-  Laurentide Ice-Sheet
-  Greenland Ice-Sheet
-  LGM maximum extent?
-  Major LGM ice-streams

-  Core Location
-  Arctic Water
-  West Greenland Intermediate Water

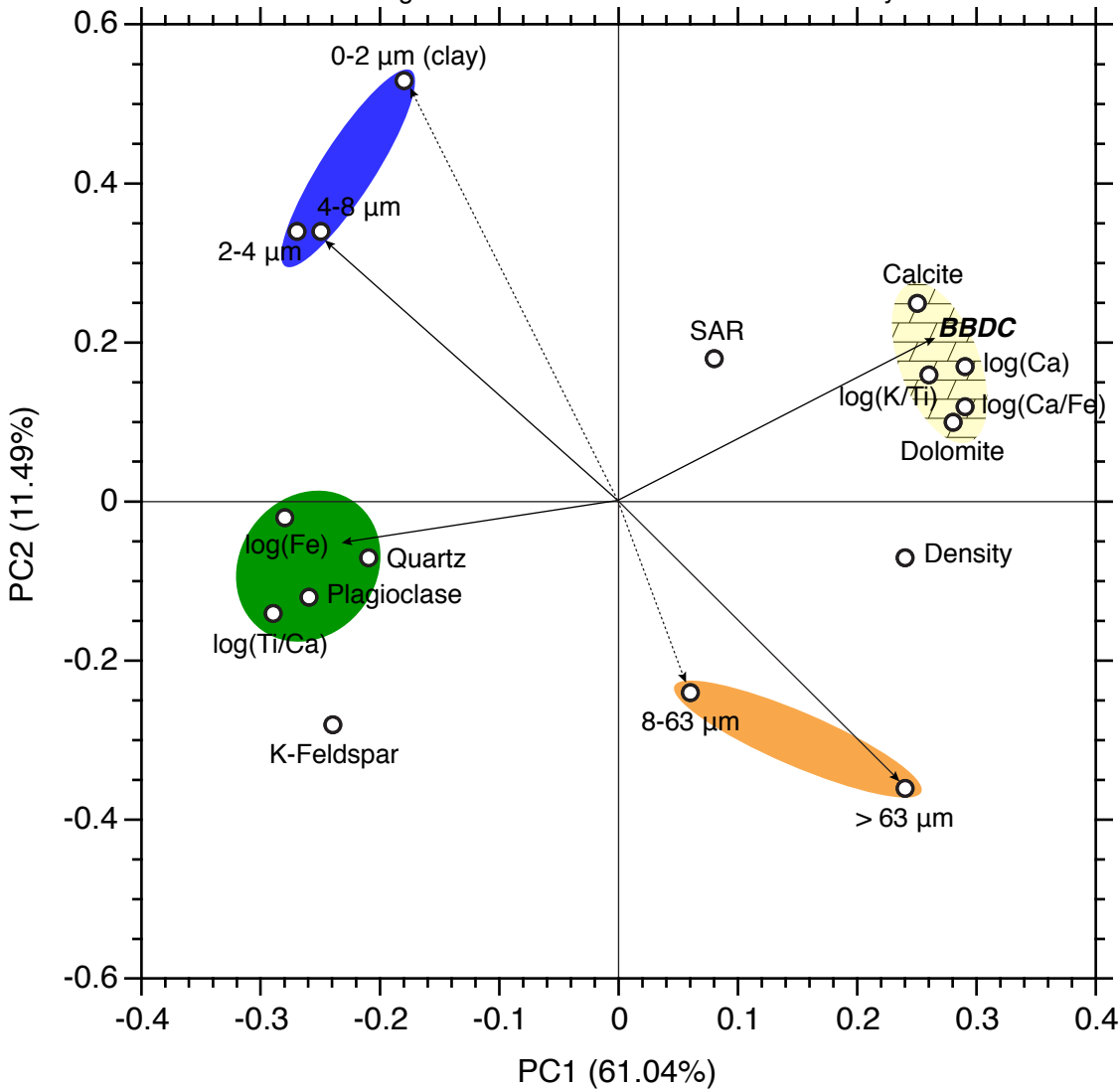


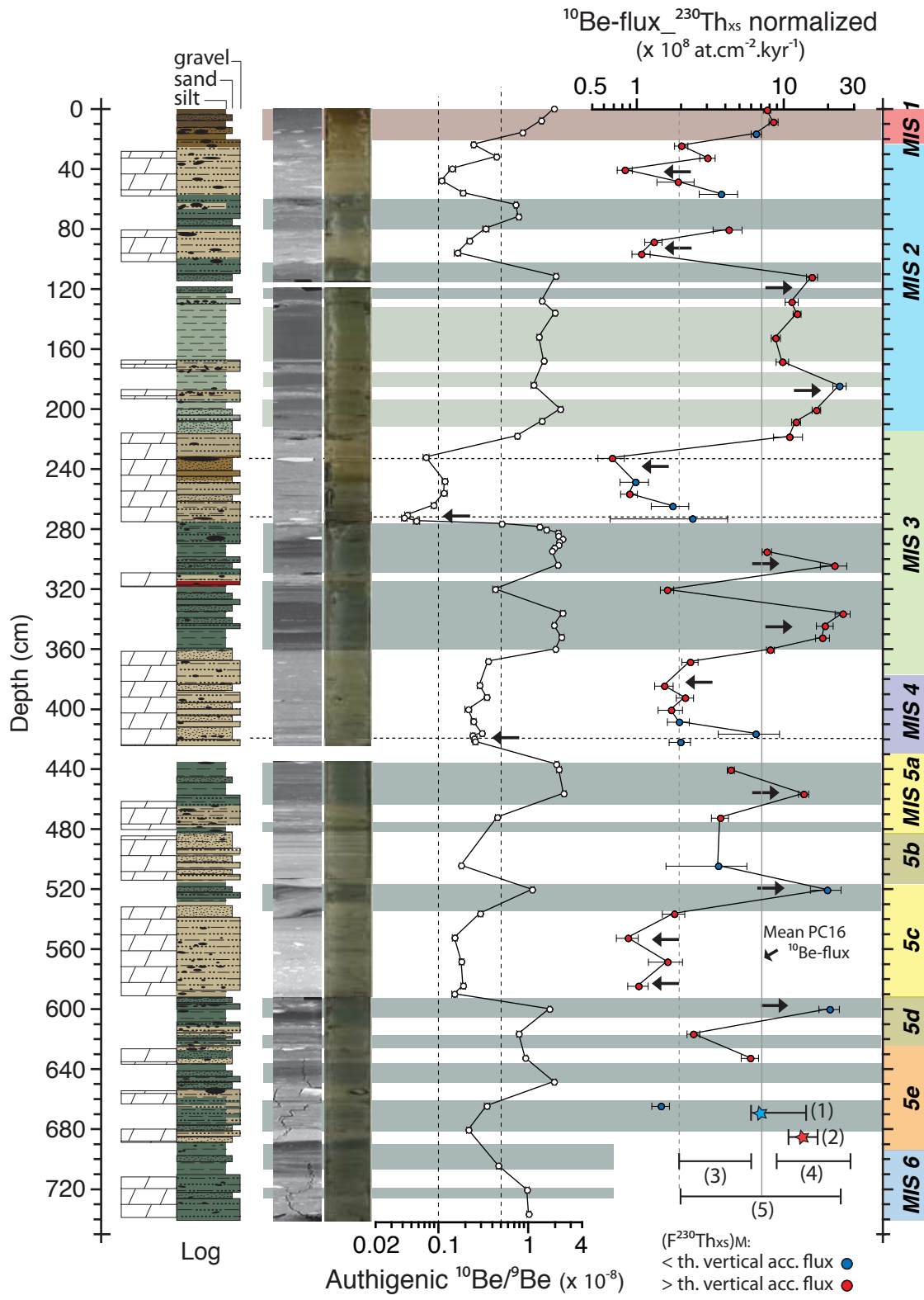


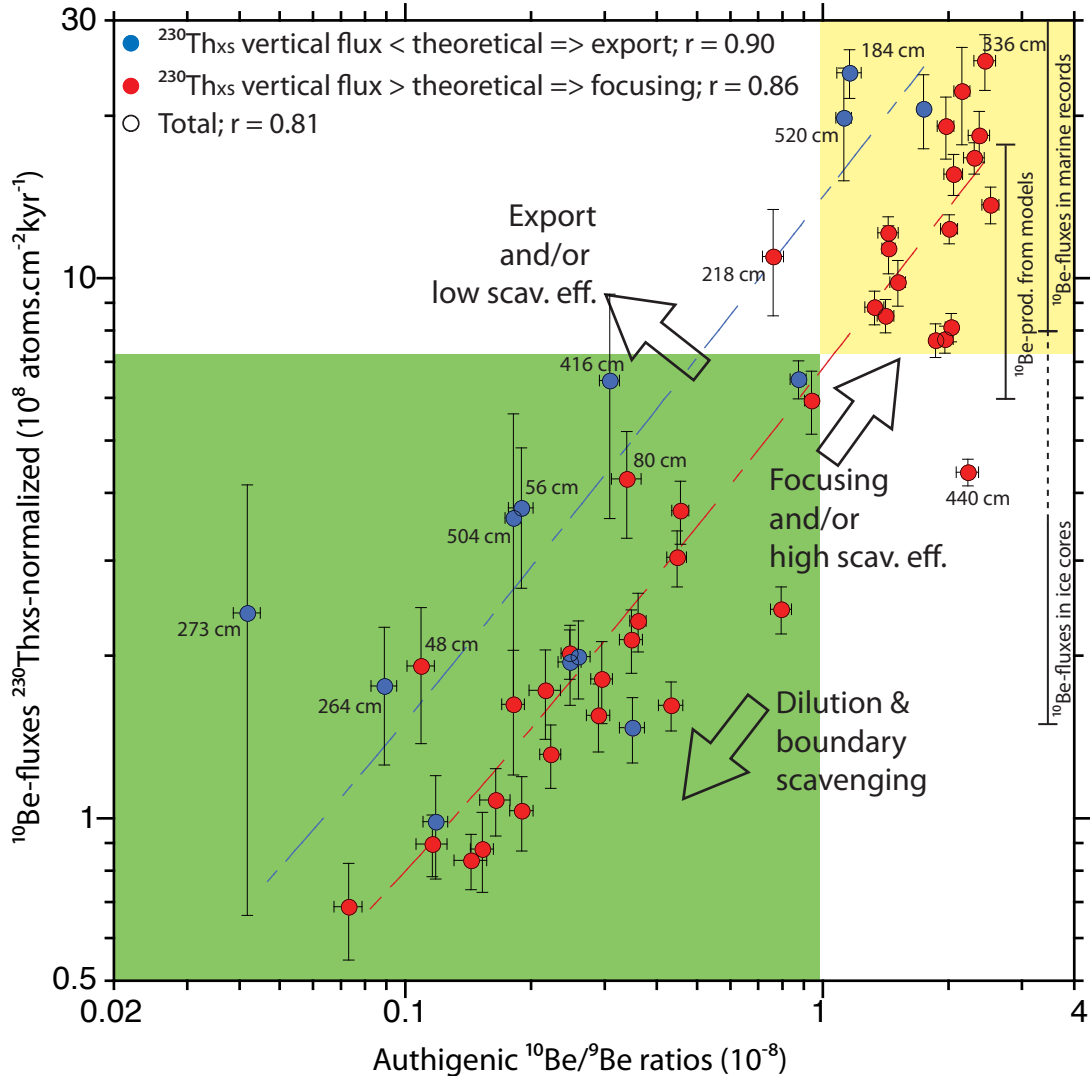


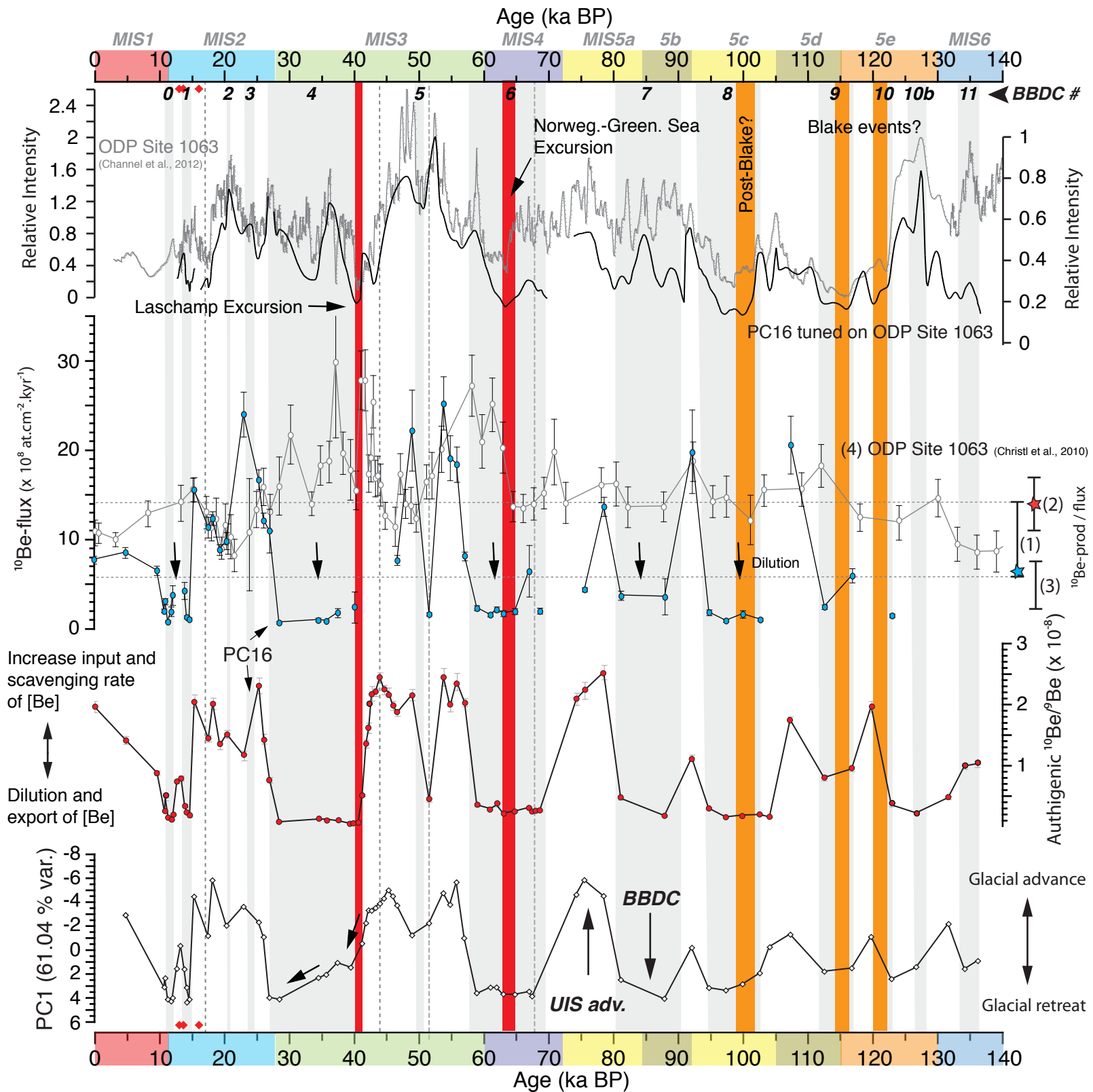
Fine sediments associated  
with extended ice margins

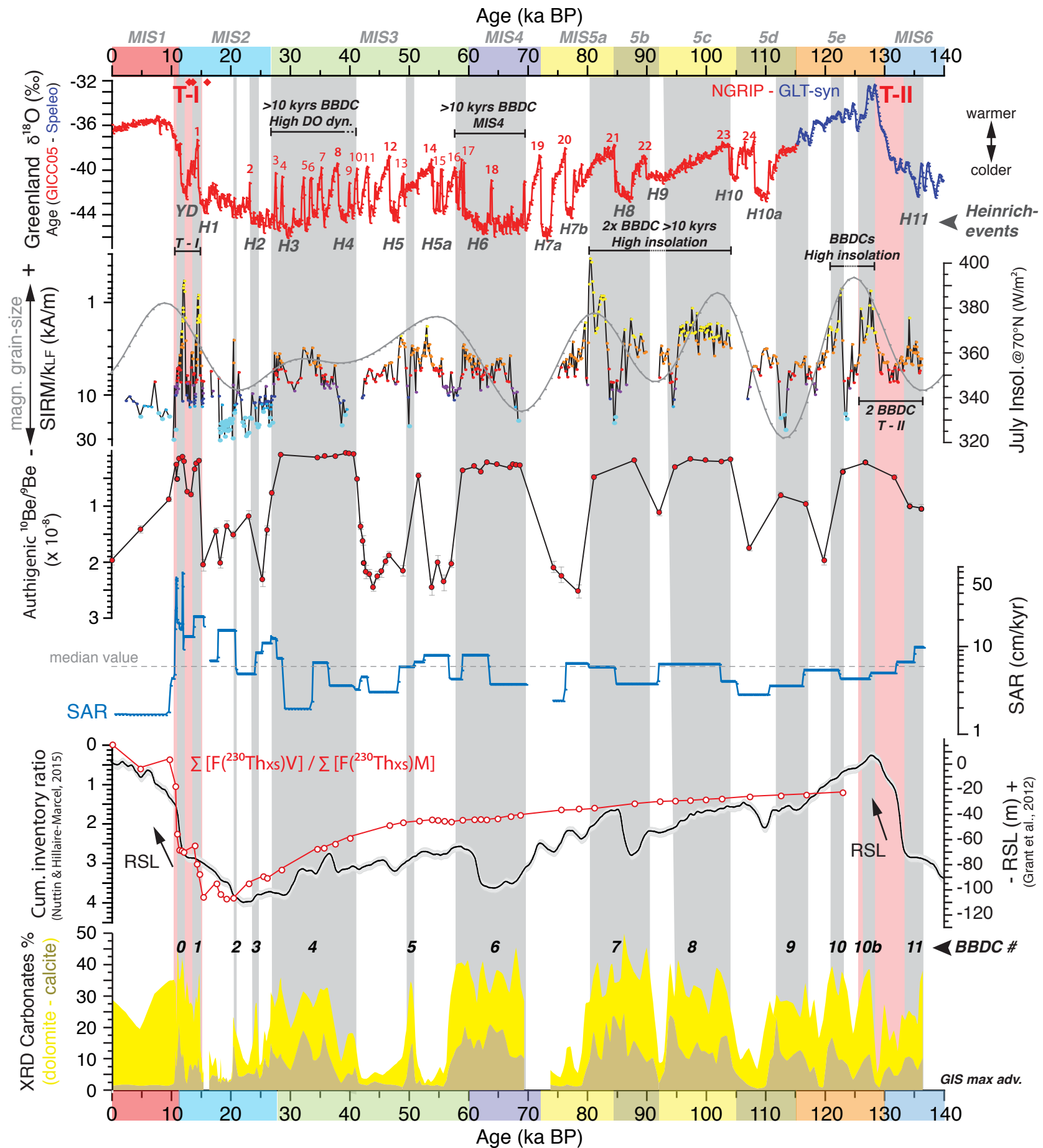
Coarse particles transported  
by IRD and sea-ice













**(a) Trans-Baffin drift****(b) Extended ice margins**